THE UNDERLYING MECHANISM OF KYNURENIC ACID-INDUCED CYTOPROTECTION AGAINST ISCHEMIA/REPERFUSION INJURY OF CARDIAC CELLS

Ph.D. Thesis

Dóra Nógrádi-Halmi, M.D.

Supervisor:

Renáta Molnár-Gáspár, Ph.D.

Doctoral School of Multidisciplinary Sciences, University of Szeged, Hungary

Department of Biochemistry

Albert Szent-Györgyi Medical School

University of Szeged

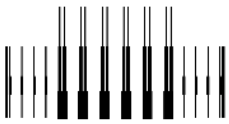

Szeged

2026

"The basic texture of research consists of dreams into which the threads of reasoning, measurement, and calculation are woven."

Albert Szent-Györgyi

List of Publications

Publications related to the subject of the thesis

I. Gáspár, R.*, **Nógrádi-Halmi, D.***, Demján, V., Diószegi, P., Igaz, N., Vincze, A., Pipicz, M., Kiricsi, M., Vécsei, L., Csont, T.: Kynurenic acid protects against ischemia/reperfusion injury by modulating apoptosis in cardiomyocytes. *Apoptosis 29, 1483–1498 (2024).* (IF (2024): 8.1, Journal Ranking: D1), *: authors contributed equally and share first authorship

II. **Nógrádi-Halmi, D**.; Erdélyi-Furka, B.; Csóré, D.; Plechl, É.; Igaz, N.; Juhász, L.; Poles, M.Z.; Nógrádi, B.; Patai, R.; Polgár, T.F.; Kiricsi, M., Vécsei, L., Gáspár, R., Csont, T.: Kynurenic Acid Protects Against Myocardial Ischemia/Reperfusion Injury by Activating GPR35 Receptors and Preserving Mitochondrial Structure and Function. *Biomolecules 5(10):1481 (2025).* (IF (2024): 4.8, Journal Ranking: Q1)

Cumulative impact factor of papers related to the thesis: **12.9**

Publications not listed in the thesis

I. Nógrádi, B., Polgár, T.F., Meszlényi, V., Kádár, Z., Hertelendy, P., Csáti, A., Szpisjak, L., **Halmi, D**., Erdélyi-Furka, B., Tóth, M., Molnár, F., Tóth, D., Bősze, Zs., Boda, K., Klivényi, P., Siklós, L., Patai, R.: ChatGPT M.D.: Is there any room for generative AI in neurology?. *PLOS ONE 19(10): e0310028. (2024).* (IF (2024): 2.6, Journal Ranking: Q1)

II. Nógrádi, B., **Nógrádi-Halmi, D.**, Erdélyi-Furka, B., Kádár Z., Csont, T., Gáspár, R.: Mechanism of motoneuronal and pyramidal cell death in amyotrophic lateral sclerosis and its potential therapeutic modulation. *Cell Death Discov*. *10, 291 (2024).* (IF (2024): 7.0, Journal Ranking: Q1)

III. Gáspár, R., Diószegi, P., **Nógrádi-Halmi, D.**, Erdélyi-Furka, B., Varga, Z., Kahán, Zs., Csont, T.: The Proteoglycans Biglycan and Decorin Protect Cardiac Cells against Irradiation-Induced Cell Death by Inhibiting Apoptosis. *Cells, 13, 883 (2024).* (IF (2024): 5.2, Journal Ranking: Q1)

IV. **Nógrádi-Halmi, D.**, Erdélyi-Furka, B., Gáspár, R., Csont, T.: Triptofán-származékok, mint lehetséges biomarkerek és terápiás célpontok egyes kardiovaszkuláris megbetegedésekben; *Cardiologia Hungarica 53: 36–224 (2023).*

V. Gáspár, R., **Halmi, D.**, Demján, V., Berkecz, R., Pipicz, M., Csont, T.: Kynurenine Pathway Metabolites as Potential Clinical Biomarkers in Coronary Artery Disease. *Front Immunol.*, *12:768560 (2022).* (IF (2022): 7.3, Journal Ranking: D1)

Total cumulative impact factor: 35

Table of Contents

List of Abbreviations

3-HK: 3-hydroxy kynurenine

3-HAA: 3-hydroxy anthranilic acid

AA: anthranilic acid

AhR: aryl hydrocarbon receptors

AMI: acute myocardial infarction

AMPA: α-amino-3-hydroxy-5-methyl-4-isoxazolepropionic acid

ATP: adenosine triphosphate

BAX: Bcl-2 associated X

Bcl-2: B-cell lymphoma 2

Bcl-XL: B-cell lymphoma extra large

CAD: coronary artery disease

CVD: cardiovascular disease

DAPI: 4,6-diamidino-2-phenylindole

DMEM: Dulbecco's Modified Eagle Medium

DMSO: dimethyl sulfoxide

D-PBS: Dulbecco's phosphate buffer solution

FBS: fetal bovine serum

Fis1: mitochondrial fission protein 1

GPR35: G-protein coupled receptor 35

IDO: indolamine-2,3-dioxygenase

IHD: ischemic heart disease

I/R: ischemia/reperfusion

KAT: kynurenine aminotransferase

KMO: kynurenine monooxygenase

KP: kynurenine pathway

KYN: kynurenine

KYNA: kynurenic acid

MFN-1/-2: mitofusin-1/-2

mtDNA: mitochondrial DNA

mtPTP: mitochondrial permeability transition pore

NAD: nicotinamide adenine dinucleotide

NADP: nicotinamide adenine dinucleotide phosphate

NMDA: N-methyl-D-aspartate

MTT: 3-(4, 5-dimethylthiazol-2-yl)-2,5-diphenyltetrazolium bromide

OPA1: optic atrophy protein 1

OXPHOS-I: Complex I-dependent oxidative phosphorylation capacity

OXPHOS-II: Complex II-dependent oxidative phosphorylation capacity

PA: picolinic acid

PBS: phosphate buffered saline

PCR: polymerase chain reaction

PFA: paraformaldehyde

QUIN: quinolinic acid

ROS: reactive oxygen species

RT: room temperature

SI/R: simulated ischemia/reperfusion

TDO: tryptophan-2,3-dioxygenase

Trp: tryptophan

1. Introduction

1.1. Cardiovascular diseases among the leading causes of death

The phrase cardiovascular disease (CVD) is an umbrella term for a broad range of conditions affecting the heart and the vascular system. Despite the substantial progress that has been introduced in the diagnosis and treatment of the underlying conditions over the past decades, CVD remain among the leading causes of mortality worldwide (*Figure 1*). According to global statistics, CVD were responsible for 27% of total deaths in 2019. The majority of these (*i.e.,* 9.1 million deaths) occurred due to ischemic heart disease (IHD), often referred to as coronary artery disease (CAD), a major entity under the CVD umbrella (*Web 1*).

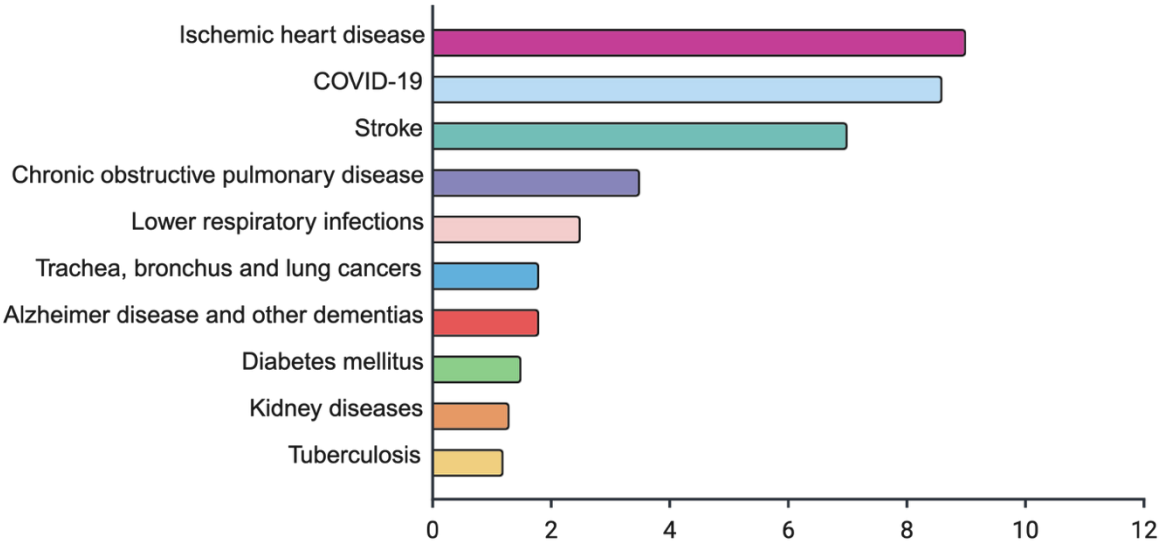

Figure 1. **Leagind causes of deaths globally in 2021**

(https://www.who.int/news-room/fact-sheets/detail/the-top-10-causes-of-death)

1.2. Ischemic heart disease and acute myocardial infarction

Ischemic heart disease is characterized by the formation of either occlusive or nonocclusive atherosclerotic plaques in the epicardial arteries. The course of the disease may include relatively stable, sometimes even clinically silent periods (*i.e.,* chronic coronary syndrome), however, acute exacerbations (*i.e.,* acute coronary syndrome) may be life-threatening [1]. These complications arise upon sudden myocardial ischemia and may present as either unstable angina or acute myocardial infarction (AMI) clinically, depending on the severity of the impairment [2].

The development of AMI relies on the obstruction of a coronary artery causing sudden decrease in the oxygen and nutrient supply to the cardiac muscle. The reduction of coronary flow initiates a variety of structural and functional abnormalities resulting in cardiomyocyte

death and subsequent impairment of cardiac functions (*e.g.,* systolic and diastolic dysfunction, reduced cardiac output, potentially culminating in heart failure) [3]. The magnitude as well as the duration of the ischemic period determines the severity of myocardial damage, therefore, the therapy of AMI heavily relies on the prevention of further mismatch in the oxygen and nutrient supply and demand via different revascularization strategies, including urgent application of antiplatelet and thrombolytic agents, percutaneous coronary intervention, or coronary bypass surgery [4]. Although the reestablishment of the coronary circulation is essential to prevent the progression of ischemia-induced cardiac tissue injuries, reperfusion has been demonstrated to damage the myocardium further, eventually leading to additional loss of functioning cardiomyocytes [5].

1.3. The pathomechanism of myocardial ischemia/reperfusion injury

The mechanism of ischemia/reperfusion (I/R)-induced cardiomyocyte damage is multifaceted, comprising various intracellular alterations. Initially, the restriction in oxygen delivery upon coronary occlusion causes a shift in the metabolism of cardiomyocytes towards anaerobic pathways, resulting in lactate buildup and subsequent intracellular acidification. Although multiple ion transporters (*e.g.,* Na^+/H^+ exchangers, Na^+/K^+ ATPases) attempt to reestablish the physiological intracellular milieu, anaerobic adenosine triphosphate (ATP) production is insufficient to maintain these active transport mechanisms, eventually leading to intracellular accumulation of Ca^{2+} and Na^+ ions (*Figure 2*) [6]. Elevation of Ca^{2+} levels may culminate in the activation of protease and hydrolase enzymes, accelerating cardiomyocyte injury through the destruction of cellular elements (*e.g.,* cytoskeletal proteins and membrane lipids), while increased Na^+ concentration may cause osmotic swelling, disrupting the plasma membrane [7]. These events collectively result in cardiomyocyte loss eventually (*Figure 2*). Upon intervention, coronary reperfusion allows the rapid restoration of ATP levels as well as the neutralization of the acidic intracellular pH, which are both essential to prevent the progression of ischemic injury. However, quick normalization of the ischemia-induced alterations may further damage the cardiac tissue as sudden exposure of damaged cardiomyocytes to oxygen promotes robust generation of reactive oxygen species (ROS) causing oxidative stress [8]. This, along with further accumulation of Ca^{2+} upon reperfusion, stimulates the opening of the mitochondrial permeability transition pore (mtPTP) [9]. Prolonged mtPTP opening collapses the mitochondrial membrane potential enabling free flow of protons across the inner mitochondrial membrane (*Figure 2*). Consequently, persistent mtPTP opening uncouples oxidative phosphorylation and depletes ATP levels again. Such

events have been reported to damage the integrity of mitochondria, causing mitochondrial swelling and membrane disruption [10]. Severely injured mitochondria are known to release their content into the cytosol, ultimately activating cell death mechanisms, triggering further loss of cardiomyocytes (*Figure 2*).

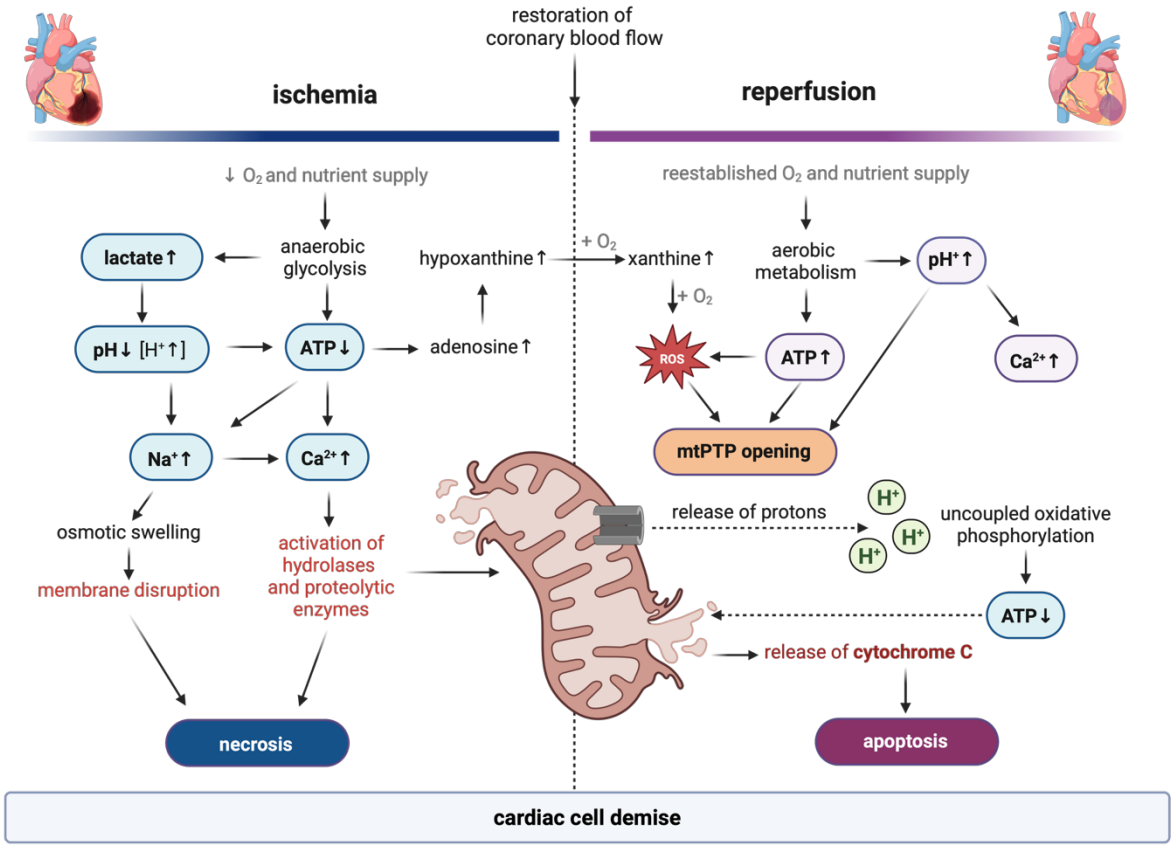

Figure 2. **Pathomechanism of ischemia/reperfusion injury.**

ATP: adenosine triphosphate, ***Ca^{2+}***: calcium, ***mtPTP***: mitochondrial permeability transition pore, ***ROS***: reactive oxygen species. *The figure was created using BioRender.com*.

1.4. Destructive mechanisms implicated in I/R-induced cardiac cell demise

1.4.1. Cell death pathways contributing to I/R-triggered cardiac cell damage

The cellular alterations induced by both ischemia and reperfusion eventually stimulate cell death through various pathways, including both uncontrolled (*e.g.,* necrosis) and regulated (*e.g.,* apoptosis, necroptosis, pyroptosis, ferroptosis or autophagy) types of cell death. These have been reported to occur along a specific sequence, with some pathways being activated simultaneously, as well as to interplay, further contributing to the complexity of I/R injury [11].

Necrosis may arise upon various non-cellular mechanisms, such as ischemia itself, ultimately leading to irreversible cardiac cell demise accompanied by swelling and consequent disruption of the plasma membrane, altering the intracellular electrolyte milieu. Necrotic cell

death is typically accompanied by inflammation, and besides playing a key role in the ischemia-induced pathologies, it is known to contribute to reperfusion injury as well [12, 13].

Other, regulated types of cell death facilitate the propagation of cardiac tissue damage during both ischemia and reperfusion. Besides the prolongation of the ischemic period, the activity of such cell death mechanisms is another key factor determining the extent of myocardial injury through affecting the survival of cardiac cells found in the viable zones adjacent to the necrotic core of the injury [14, 15]. Understanding these mechanisms and their interactions is pivotal for the future development of cardioprotective strategies, aiming to improve the survival of cardiomyocytes undergoing I/R.

Along the course of a series of adaptive and destructive mechanisms activated by I/R, autophagy operates as a survival mechanism initially, aiming to cope with hypoxia and altered energy metabolism. It sustains intracellular stability through the degradation of damaged organelles and macromolecules. Both prolongation of the ischemic period and sudden re-entry of oxygen upon revascularization, however, cause a shift in its process, ultimately leading to autophagic cell death [16]. Meanwhile, myocardial cells exposed to ischemia release inflammatory mediators, that have been described to aggravate inflammasome activation and caspase-1 mediated pyroptosis. Although pyroptosis has been reported to show beneficial features during the early phases of I/R, throughout latter stages, it facilitates the release of further mediators propagating inflammation, that can directly activate the process of controlled necrosis, often referred to as necroptosis [16, 17]. These two mechanisms are known to overlap, as well as to share some mechanistic similarities [18]. Importantly, both have been reported to interplay with the process of apoptotic cell death [19]. Apoptosis is another regulated form of cellular demise, accompanied by characteristic morphological and biochemical hallmarks [20]. Its process is known to be initiated along either of two well-characterized pathways, the extrinsic and intrinsic apoptotic pathways (*Figure 3*). Both of these are governed by multiple cysteine protease enzymes called caspases, that are present in their zymogen form and undergo proteolytic cleavage upon apoptotic stimuli, yielding protease activity [21]. Importantly, caspase activation occurs along a strict order, with extrinsic and intrinsic initiator caspases (*e.g.,* caspase-8, and -9) being activated first (*Figure 3*). Nutrient deprivation, inadequate oxygen supply, in line with oxidative stress cause mitochondrial damage, thereby activating intrinsic apoptosis initiation. Besides enhanced Ca^{2+} accumulation, disruption of the balance between the expression of various mitochondrial membrane proteins showing either pro- or antiapoptotic properties contributes to the mitochondrial injuries. For example, increased presence of proapoptotic Bcl-2-associated-X (BAX) relative to the amount of antiapoptotic B-cell

lymphoma 2 (Bcl-2) and B-cell lymphoma extra-large (Bcl-XL) proteins impairs the integrity of the mitochondrial membrane, switching on the intrinsic apoptotic program through cytochrome-C release and consequent activation of caspase-9. On the other hand, propagation of oxidative stress, as well as release of inflammatory cytokines have been reported to stimulate death receptors (*e.g.*, tumor necrosis factor and Fas receptors), inducing the extrinsic program through caspase-8 activation (*i.e.*, procaspase-8 to caspase-8 conversion). The extrinsic and intrinsic pathways converge at the level of executioner caspases (*e.g.,* caspase-3, caspase-7), which are known to trigger endonuclease-mediated chromosomal degradation as well as disruption of the cytoskeletal system, thereby damaging intracellular transport and signal transduction mechanisms [21, 22]. These molecular events lay behind the development of morphological hallmarks of apoptosis, including cell shrinkage, chromatin condensation, apoptotic body formation and membrane blebbing [22].

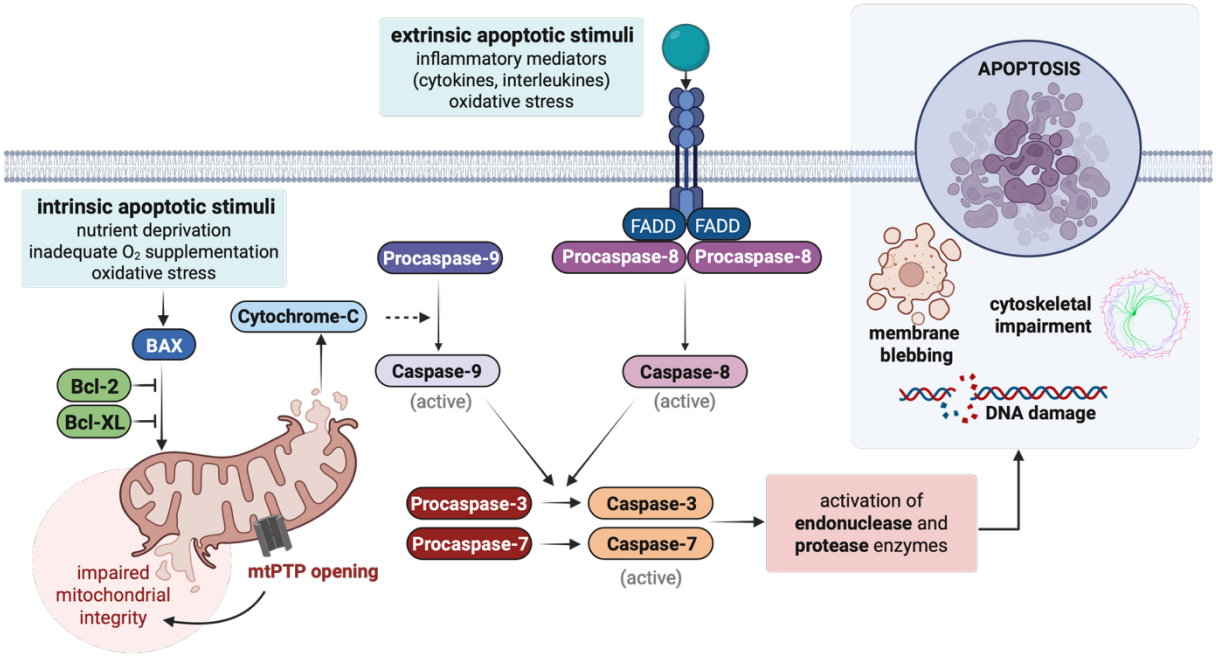

Figure 3. **Mechanism of I/R-induced apoptotic cell death.**

BAX: *Bcl-2 associated X,* ***Bcl-2****: B-cell lymphoma 2,* ***Bcl-XL****: B-cell lymphoma extra-large. The figure was created using BioRender.com.*

Importantly, the process of apoptosis has been reported to contribute significantly to I/R-triggered myocardial injuries [23]. Programmed cell death has been shown to proceed slowly during the ischemic period, often culminating in necrotic cell death afterwards due to energy depletion. However, it has been reported to intensify upon reperfusion through restoring energy required for the completion of apoptosis [24]. During reperfusion, apoptosis is thought to be among the most significant cell death types, determining the extent of myocardial injuries [25, 26]. It also has been reported that cardiac cells showing signs of apoptosis are present in

myocardial areas neighboring the zones exposed to I/R. These apoptotic cardiomyocytes have been detected not only in the remote myocardial tissue (*i.e.,* shortly after the ischemic insult), but months later as well, suggesting that apoptosis plays fundamental roles in cardiac remodeling as well as in the development of heart failure as a long-term complication of AMI [25]. These, along with the fact that programmed cell death occurs along a distinct series of biochemical reactions, raises the potential for the development of cardioprotective strategies targeting key apoptotic events, thereby suppressing programmed cell death and improving the survival of cardiac cells exposed to I/R.

1.4.2. The role of mitochondrial injuries in I/R-induced cardiac cell damage

Ischemia/reperfusion is known to impair mitochondria severely, disturbing mitochondrial dynamics, structure, as well as deteriorating mitochondrial functions [27, 28]. Over the past years, it has become apparent that the degree of mitochondrial damage is a determinative factor during the development of myocardial I/R injuries, showing a fundamental impact on overall cardiomyocyte loss, as well as on the severity of consequent functional impairments [29]. Along the course of I/R-triggered mitochondrial deterioration, ischemia-induced electron transport chain injuries have been reported to occur first, priming the mitochondria for further damage aggravated by the reintroduction of oxygen upon reperfusion [29]. During the early stages of reperfusion, primed mitochondria have been demonstrated to govern the propagation of cellular injuries through massive release of ROS and dysregulation of Ca^{2+} homeostasis. Oxidative stress and accumulation of Ca^{2+} are both known to alter permeation, causing mtPTP opening, followed by the release of matrix constituents into the cytosol [29, 30]. In addition, mtPTP opening has been reported to increase the colloid-osmotic pressure within the matrix, ultimately resulting in mitochondrial swelling [31]. These mechanisms may trigger either necrotic or programmed cardiac cell death, depending on the severity of mitochondrial impairments as well as on the degree of energy depletion.

Importantly, various adaptive mechanisms, collectively termed as mitochondrial quality control mechanisms, operate in cells to maintain mitochondrial homeostasis by the removal of dysfunctional mitochondria and restoration of proper architecture (*Figure 4*) [32]. Fusion and fission, for example, have both been demonstrated to affect the arrangement of the mitochondrial network, as well as the morphology of individual mitochondria with consequent effects on functional parameters [31]. Fusion has been reported to repair reversibly damaged mitochondrial fragments by connecting them to neighboring healthy mitochondria, thereby allowing the exchange of matrix constituents [33]. During the process of fusion, dynamin-

related GTPases, such as mitofusin-1 and -2 (MFN-1, MFN-2) join the outer membranes, while optic atrophy protein 1 (OPA1) is responsible for the fusion of the inner membranes (*Figure 4*). Fission, on the other hand, is responsible for the division of mitochondrial aggregates. It is known to create two daughter organelles: a regenerated one showing higher membrane potential and fusion capacity, and a defective one degraded later on by mitophagy (*Figure 4*) [33]. Besides exhibiting adaptive potentials, aiming to cope with the I/R-induced impairments, fusion and fission are both important contributors to various pathologies as well [34]. Pathological fusion has been demonstrated to cause cellular demise through MFN-2-mediated activation of caspase-9 resulting in intrinsic apoptosis initiation (*Figure 4*) [35]. Excessive fission of mitochondria, on the other hand, has been reported to promote mitochondrial DNA (mtDNA) damage, reducing the transcription of genes encoding respiratory complex components, ultimately leading to decreased respiratory capacities, depleted energy production and increased mitochondrial ROS release [27, 32]. In addition, over-enhanced fission prolongs mtPTP opening, thereby contributing to intrinsic apoptosis initiation (*Figure 4*) [27].

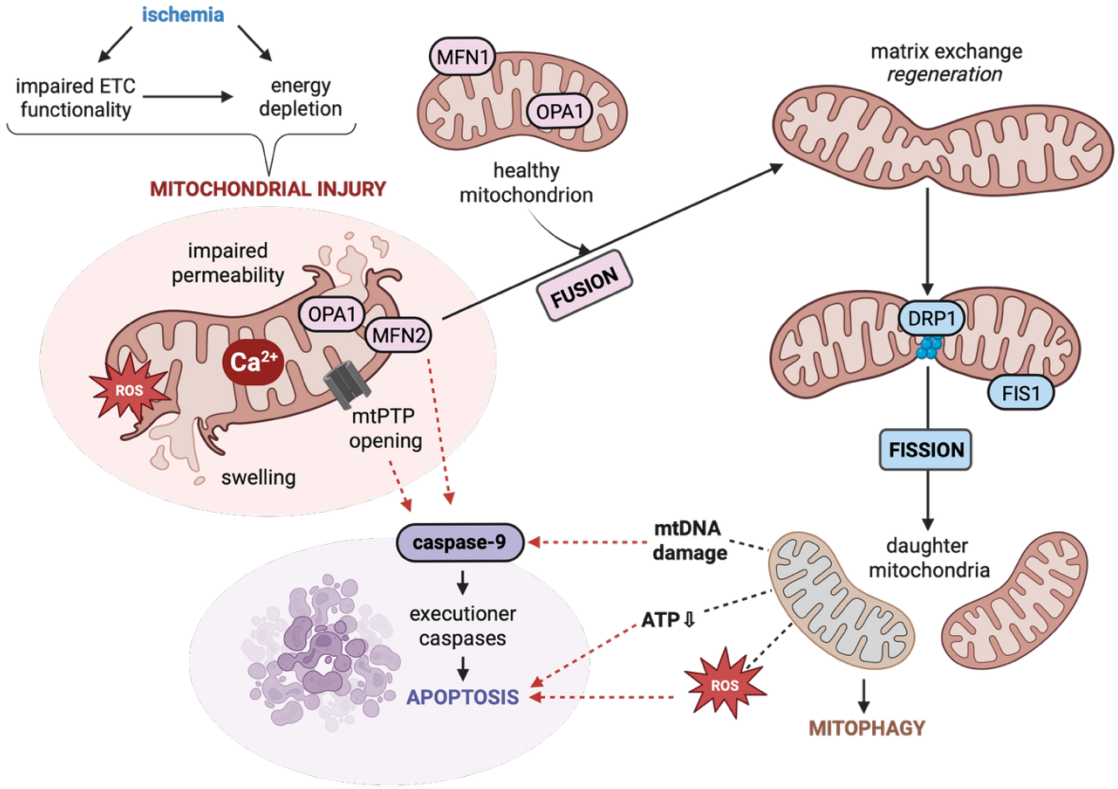

Figure 4. **Adaptive and pathological features of mitochondrial fusion and fission.**

***ETC**: electron transport chain, **ROS**: reactive oxygen species, **MFN1**: Mitofusin-1, **MFN2**: Mitofusin-2, **OPA-1**: optic atrophy protein 1, **mtPTP**: mitochondrial permeability transition pore, **DRP**: dynamin-related protein, **FIS1**: mitochondrial fission protein 1.*
The figure was created using BioRender.com.

Considering that mitochondria seem to play a fundamental role in the development of I/R-induced myocardial pathologies, targeting the preservation of mitochondrial integrity may be another promising approach along the development of novel cardioprotective agents.

1.5. Attempts to rescue cardiac cells: conditioning strategies aiming to reduce ischemia/reperfusion injury

Over the past decades, multiple cardioprotective strategies have been developed to protect the cardiac tissue against the harmful effects of I/R. These methods are known to induce adaptive cellular and molecular mechanisms, thereby improving the tolerance of the myocardial tissue against ischemia. Ischemic conditioning has been one of the first methods described to trigger such effects. This approach is known to protect cardiac cells through applying brief, alternating episodes of non-lethal ischemia and reperfusion either before, during or immediately after a sustained ischemic insult, known as pre-, per- or postconditioning, respectively. Besides being applied to the myocardial tissue itself, the conditioning stimuli may be directed to distant organs, triggering remote ischemic conditioning [36]. Uncovering the molecular mechanisms laying behind the protective effects of such approaches supported the identification of signaling pathways, the modulation of which may induce cardioprotective programs. Attempts to induce these mechanisms via exogenous administration of compounds showing protective potential, often referred to as pharmacological conditioning, have not achieved substantial cardioprotection in clinical settings to date [36]. Nevertheless, identification and analysis of further agents that could trigger cardioprotective mechanisms, carrying the potential to conduct successful pharmacological conditioning is of great importance and may contribute to the development of future therapeutic strategies aiming to improve the clinical outcomes in CAD patients.

1.6. Tryptophan and the kynurenine pathway

Tryptophan (Trp) is an indole structure, carrying the largest molecular weight among the 20 proteogenic amino acids. Its average tissue concentration, however, is known to be the lowest, with Trp being the least abundant amino acid in proteins. It belongs to the group of essential amino acids, which are obtained solely through dietary intake. The optimal daily Trp intake is known to be around 3.5–6.0 mg/body weight kilograms for adults [37]. Common sources involve chicken, turkey, tuna fish, various dairy products (*e.g.,* milk, cheese), oats, banana, peanuts and chocolate [37]. Although less then 1% of the supplied Trp is utilized for protein synthesis, it still has a fundamental role during translation, being a rate-limiting factor due to its relatively low availability [38]. Nevertheless, the majority of Trp is metabolized through

various pathways either before or after its absorption from the intestines. Gut microbiota have been reported to convert a small fraction of dietary Trp to indole derivatives, which have the potential to influence the expression of various pro- and anti-inflammatory cytokines in the gastrointestinal tract [39]. Trp absorbed from the gut, however, is converted further along either the 5-hydroxytryptamine or kynurenine pathways, generating various biologically active compounds. While only approximately 1% of Trp is utilized for serotonin and melatonin production through the 5-hydroxytryptamine pathway, the majority of dietary Trp, nearly 95%, is known to be metabolized along the kynurenine pathway (KP), producing multiple compounds collectively termed as kynurenines, as well as niacin (*i.e.,* vitamin B3), nicotinamide adenine dinucleotide (NAD) and nicotinamide adenine dinucleotide phosphate (NADP) [37, 40].

The degradation of Trp along the KP is driven by the rate-limiting conversion of Trp to *N*-formyl-*L*-kynurenine catalyzed by either tryptophan-2,3-dioxygenase (TDO) or indoleamine-2,3-dioxygenase-1 and -2 (IDO-1, IDO-2) enzymes (*Figure 5*). TDO is primarily expressed in the liver and accounts for approximately 90% of Trp catabolism [40]. IDO-1/-2 enzymes, on the other hand, have been reported to be present at multiple extrahepatic locations, including, but not limited to the heart, lung and small intestines. Despite the fact that they metabolize less Trp, they are considered quite significant as they initiate the generation of various compounds exhibiting either physiological or pathophysiological roles [41, 42]. Along the KP, *N*-formyl-*L*-kynurenine is then hydrolyzed to *L*-Kynurenine (KYN), a core compound of the pathway, which can be further converted along three branches yielding either 3-hydroxykynurenine (3-HK), anthranilic acid (AA) or kynurenic acid (KYNA) (*Figure 5*). Under physiological circumstances, the majority of KYN is oxidated by kynurenine monooxygenase (KMO) to 3-HK to initiate a pathway yielding NAD and NADP. Along this route, 3-HK is first hydrolyzed to 3-hydroxyanthranilic acid (3-HAA), which is then converted to 2-amino-3-carboxymuconate semialdehyde that serves as a precursor of picolinic acid (PA) and quinolinic acid (QUIN). Finally, QUIN is utilized to produce NAD and NADP through a multistep process. The kynureninase-catalyzed hydrolysis of KYN to AA is less abundant, but still significant due to potential beneficial roles exhibited by AA and its derivatives [43, 44]. The third major pathway of KYN metabolism is the formation of KYNA through the transamination of KYN catalyzed by either of the four known kynurenine aminotransferase (KAT) isoenzymes (*Figure 5*), expressed at various locations throughout the human body, involving the heart [45].

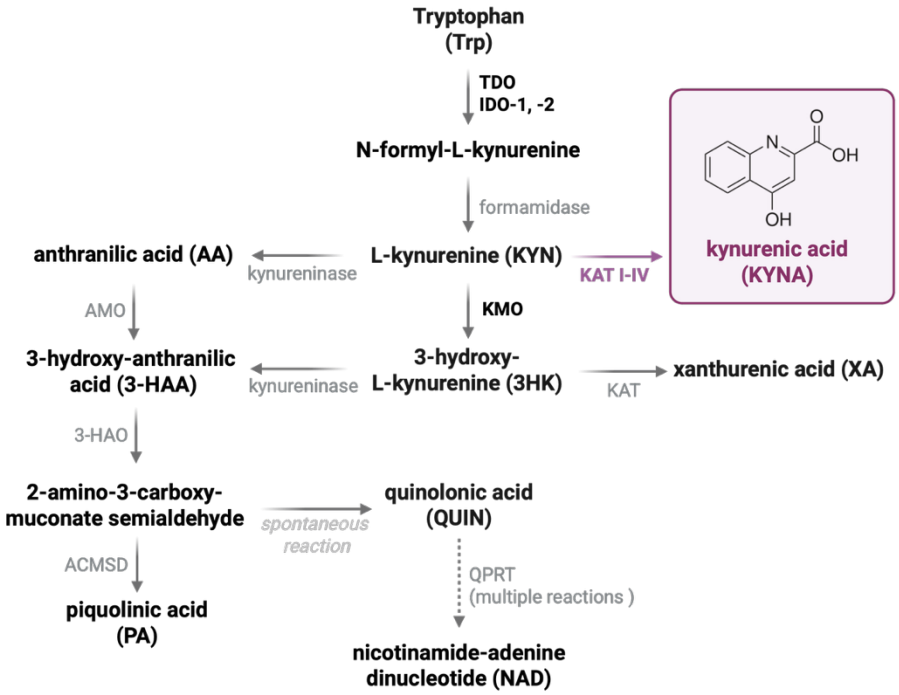

Figure 5. **Metabolism of tryptophan along the kynurenine pathway.**

***Trp**: tryptophan, **TDO**: tryptophan-2,3-dioxygenase, **IDO-1 and -2**: indolamine-2,3-dioxygenase-1 and -2, **KAT**: kynurenine aminotransferase, **AMO**: anthranilate-3-monooxygenase, **3-HAO**: 3-hydroxyanthranilate oxidase, **ACMSD**: aminocarboxymuconate semialdehyde decarboxylase, **QPRT**: quinolinate phosphoribosyltransferase. The figure was created using www.BioRender.com.*

1.7. Kynurenic acid: chemical characteristics and known effects

The effect of kynurenine compounds, including KYNA, have been extensively studied over the past decades. Most of these investigations assessed the role of altered release of kynurenines in the development and progression of various neurological conditions. Although certain compounds, such as 3-HAA or QUIN have been reported to exhibit neurotoxic effects, other kynurenines, involving KYNA, have been shown to exert neuroprotective properties in multiple neurodegenerative conditions and cerebrovascular diseases [46, 47]. Besides interactions in the nervous system, kynurenines have been reported to execute pivotal roles in the periphery as well, and are known for their immunomodulatory features, for instance [48].

KYNA is a polar compound present in various bodily fluids and tissues, including but not limited to blood, cerebrospinal fluid, bile, urine, the intestines and the heart [49]. Serum concentration of KYNA has been reported to range between 30-50 nM in healthy individuals [49]. Due to its chemical features, it does no cross biological membranes easily, instead, it applies transporters or acts through binding to cell surface receptors. KYNA has been shown to antagonize various inotropic glutamate receptors, including N-methyl-D-aspartate (NMDA), α-

amino-3-hydroxy-5-methyl-4-isoxazolepropionic acid (AMPA), and kainate receptors. On the other hand, other receptors, such as G-protein coupled receptor 35 (GPR35) and aryl hydrocarbon receptors (AhR) are known to be stimulated when bound to KYNA [50].

Through the modulation of these receptors, KYNA has been shown to affect the expression and/or activity of various molecules governing intracellular signaling pathways, including, but not limited to phosphoinositide 3-kinase (PI3K)/protein kinase B (Akt), extracellular signal regulated kinases (ERK)-1/-2, mitogen activated protein kinase (MAPK), cyclin-dependent kinase inhibitor p21, retinoblastoma protein, as well as multiple interleukins and chemokines [48, 51]. Along these interactions, KYNA carries the capacity to impact the balance between cell survival and death, as well as to exert anti-inflammatory, immunosuppressive [52], antinociceptive [53] and antiproliferative effects [51]. Additionally, KYNA has been reported to improve energy metabolism [54, 55], as well as to suppress calcium mobilization with subsequent amelioration of inflammasome activation [56]. Considering that calcium homeostasis plays a fundamental role in the determination of cell survival, this effect may contribute to further aspects of its cytoprotective potential (*e.g.*, it may contribute to plausible antiapoptotic effects). Importantly, besides modulating multiple signaling pathways, KYNA has been reported to show antioxidant capacity as well, along which KYNA administration has been reported to attenuate the hypoxia/ischemia-induced increase in ROS production and glutathione levels [57, 58]. These molecular mechanisms are thought to contribute to the protective potential of KYNA in various tissues. Alterations in signal transduction aggravated by NMDA-antagonism have been described to play a key role in the KYNA-induced neuroprotection in both neurodegenerative and cerebrovascular disease models [59–62]. GPR35 receptor agonism, on the other hand, has been demonstrated to mediate the effects of KYNA on Ca^{2+} homeostasis, as well as its anti-inflammatory, immunosuppressive and antinociceptive features [48, 53, 56].

Outside of the nervous system, KYNA has been reported to provide protection against intestinal [63], endometrial [64] and liver injuries [65, 66]. Importantly, the protective effects of KYNA against I/R-induced neuronal injuries have been corroborated in the cardiovascular system too. To date, multiple investigations have confirmed that KYNA exerts protective effect in cardiomyocytes against I/R [67–69]. In these settings, enhanced endogenous KYNA production has been associated with the cardioprotective effect of remote ischemic conditioning [68], and conservation of energy conservation [69]. Nevertheless, the thorough mechanism of action (*i.e.,* additional aspects of cytoprotection) has not been elucidated yet.

2. Objectives

The aim of the present thesis was to explore key intracellular pathways laying behind the previously uncovered cardiocytoprotective effect of KYNA in the setting of SI/R. The effects of KYNA were tested on H9c2 cardiomyoblasts exposed to an *in vitro* model of AMI. The study aimed to answer the following specific questions:

1) Does KYNA administration ameliorate the proapoptotic shift aggravated by SI/R?
    a. Are morphological hallmarks of apoptosis in cardiac cells exposed to SI/R attenuated by KYNA treatment?
    b. Does KYNA application modulate apoptotic signaling?
    c. Does KYNA prevent camptothecin-induced cell death, directly affecting the propagation of apoptosis?
2) Does KYNA treatment influence the integrity of mitochondria in cardiac cells undergoing SI/R?
    a. Whether KYNA administration preserves mitochondrial ultrastructure?
    b. Does KYNA application impact the functionality of mitochondria?
3) Which target receptors are implicated in the KYNA-mediated cardiocytoprotection: are GPR35 receptors fundamental contributors to the KYNA-derived beneficial effects?
    a. Whether KYNA prevents SI/R-induced cell death in absence of GPR35 receptor agonism?
    b. Does selective GPR35 stimulation, using an agonist other than KYNA, improve the survival of cardiac cells exposed to SI/R as well?

3. Methods

3.1. Cell culture

H9c2 cardiomyoblasts (ATCC; St. Louis, MO, USA; RRID: CVCL_0286) were cultured in Dulbecco's modified Eagle's medium (DMEM; Biosera, Cholet, France, Cat#LM D1108) supplemented with 10% v/v fetal bovine serum (FBS; Biosera, Cat#FB-1090), 1% v/v glutamine (Sigma-Aldrich, St. Louis, MO, USA, Cat#G7513) and 1% v/v antibiotic/antimycotic cocktail (Biosera; Cat#XC-A4110). Cells were maintained in 25 and 75 cm^2 tissue culture flasks. Cardiomyoblasts were seeded at a density of 4 x 10^3 cells/well into 96-well plates for viability measurements, 1.5 x 10^4 or 2 x 10^4 cells/well into 24-well plates containing glass coverslips for mitotracking and immunocytochemistry, and 9 x 10^5 cells/well into 6-well plates for the assessment of apoptotic membrane blebbing. To prepare samples for western blotting and electron microscopy, as well as to collect RNA samples for polymerase chain reaction (PCR), cells were cultured in 75cm^2 flasks. Cells were subjected to the different experimental protocols 2 days after cell seeding.

3.2. Experimental protocols

3.2.1. Simulated ischemia/reperfusion model

To mimic AMI *in vitro*, cardiac cells were subjected to simulated ischemia, followed by simulated reperfusion (*Figure 6*). A glucose-free hypoxic solution (119 mM NaCl, 5.4 mM KCl, 1.2 mM NaH_2PO_4, 0.5 mM $MgCl_2$, 5 mM HEPES, 1.3 mM $MgSO_4$, 0.9 mM $CaCl_2$, 20 mM Na-lactate and 0.1% BSA, pH 6.4) was prepared and applied throughout the ischemic period. Before the experiments, nitrogen gas was introduced to the hypoxic solution, followed by sonication to minimize its oxygen-content. To prevent the re-entry of oxygen, cell cultures maintained under hypoxic solution supplemented with KYNA or its vehicle were placed into a hypoxic chamber (0.4% O_2; 95% N_2, 5% CO_2, 37°C) for the entirety of simulated ischemia (*i.e.*, 6 hours). To mimic reperfusion, hypoxic solution was replaced with 10% v/v FBS-containing medium supplemented with the corresponding treatments, followed by the placement of cell cultures into a standard CO_2 incubator (5% CO_2, 37°C) for 2 hours. A control group of cells was kept under normoxic conditions during the protocol (*i.e.*, cells were maintained in a standard CO_2 incubator, under normoxic solution and medium in parallel with simulated ischemia and simulated reperfusion, respectively).

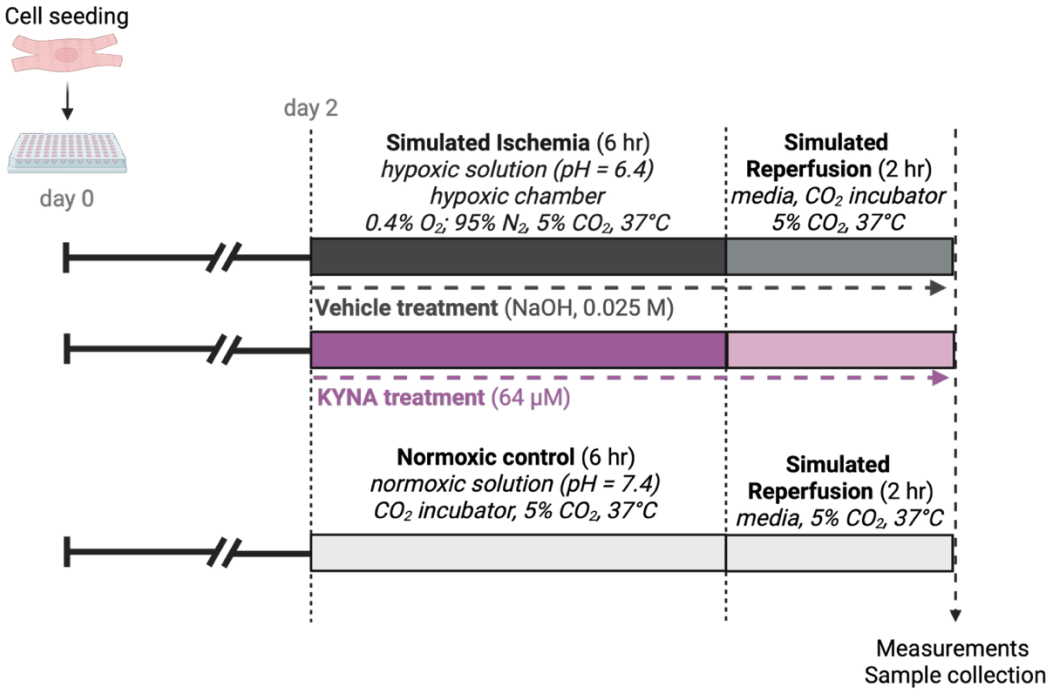

Figure 6. **Experimental protocol of simulated ischemia/reperfusion.**

3.2.2. Camptothecin-induced apoptotic cell death model

To investigate whether the protective effect of KYNA involves direct antiapoptotic mechanisms, we assessed the potential effects of KYNA administration on apoptosis-induced cellular demise. Camptothecin (Cell Signaling Technology, Danvers, MA, USA, Cat#13637) was applied at a concentration of 10 µM to induce programmed cell death, dissolved in DMEM supplemented with 1% v/v FBS, for 24 hours. H9c2 cells were pretreated with 64 µM KYNA or its vehicle before subjection to camptothecin for 24 h. The corresponding KYNA/vehicle treatments were maintained during the 24 hours of camptothecin exposure. At the end, 3-(4,5-dimethylthiazol-2-yl)-2,5-diphenyltetrazolium bromide (MTT) assay was performed to measure cell viability.

3.3. Treatments

3.3.1. Kynurenic acid treatment

To provide KYNA treatment solutions, a 10 mM stock solution was prepared by the dissolution of KYNA powder (Sigma-Aldrich, Cat#K3375) in 0.025 M NaOH. The pH of the stock solution was adjusted to 7.38-7.42 using 1 M hydrogen-chloride. To investigate the underlying mechanism of the KYNA-induced cytoprotection against SI/R, the stock solution was further diluted in either hypoxic solution (*i.e.*, during simulated ischemia) or 10% v/v FBS-containing medium (*i.e.*, during simulated reperfusion) to achieve the desired concentration of 64 µM that has been previously shown to protect cardiac cells against SI/R injury [70].

3.3.2. Treatments with agents modulating GPR35 receptor activity

To achieve GPR35 receptor activation, cardiac cells exposed to SI/R were treated using Zaprinast at a concentration of 100 μM based on literature data [71, 72]. First, a 100 mM Zaprinast stock solution was prepared by the dissolution of Zaprinast powder (Sigma-Aldrich, Cat#Z0878) in dimethyl sulfoxide (DMSO; Serva, Heidelberg, Germany, Cat#20385.01), which was then further diluted in either hypoxic solution or 10% v/v FBS-containing medium to achieve the desired concentration of 100 μM. To test the effects of GPR35 receptor inhibition, cells undergoing SI/R received CID2745687 treatment. To prepare treatment solutions, a 10 mM stock solution was provided by the dissolution of CID2745687 powder (Tocris Bioscience, Cat#4293) in DMSO. The stock solution was then further diluted in either hypoxic solution or 10% v/v FBS-containing medium to achieve the desired treatment concentration of 1 μM. To test whether KYNA maintains its protective potential with GPR35 receptors being antagonized, combined treatments (*i.e.,* 64 μM KYNA + 1 μM CID2745687) were administered. Importantly, the DMSO-content was kept under 0.2 % v/v in all applied treatment solutions to avoid potential DMSO-related cardioprotective effects. Final DMSO concentrations were 0.1% v/v and 0.002% v/v along Zaprinast and CID2745687 treatments, respectively.

3.4. Investigation of apoptotic membrane blebbing

To examine if KYNA modulates the SI/R-induced alterations in apoptosis, cells were seeded into 6-well plates and subjected to the experimental protocol with or without KYNA treatment to assess the propagation of apoptotic membrane blebbing, belonging to the morphological hallmarks of programmed cell death. After the protocol, cells were washed with warm PBS, collected using 0.25% trypsin-EDTA solution (Corning, cat#25-053-Cl, 5 min, 37 °C), and centrifuged (400 x g) for 5 min at room temperature (RT). Cell pellets were resuspended in media containing 10% v/v FBS and placed onto slides. A Leica DMi1 inverted light microscope (Leica Mycrosystems, Wetzlar, Germany) was applied to capture 5-8 fields of view per sample. An observer counted and categorized all visualized cells in a blinded manner according to the morphological characteristics of the different stages of apoptotic membrane blebbing using Image J Software with cell counter plugin (National Institutes of Health, Bethesda, MD, USA). Briefly, cells showing healthy or mildly affected morphology (*i.e.,* rounded, intact cell contour or minor alterations in membrane refraction) were grouped into Stage 1 and Stage 2, respectively. Cells showing signs of advanced apoptotic blebbing were classified into Stage 3-5 according to the following criteria: cells with peripheral circular bulges were considered to show cell surface blebbing (Stage 3), while further progression indicated dynamic blebbing

(Stage 4). Finally, cells with critically altered shape were grouped into the stage of final fragmentation (Stage 5) [73–76]. After counting, the number of cells in each stage was expressed as percentage of the total cell count on each field of view.

3.5. Assessment of nuclear morphology

To assess the ratio of cells exhibiting apoptotic nuclear morphology, cells were seeded into 24-well plates containing glass coverslips at a density of $2x10^4$ cells/well and exposed to SI/R with or without KYNA treatment. After the protocol, cells were fixed in 4% paraformaldehyde (PFA, Alfa Aesar, Haverhill, MA, USA, Cat#30525-89-4) (20 min, room temperature (RT)) and permeabilized using 0.3% Triton-X-100-containing PBS (20 min, RT). Cell nuclei were then visualized using 4,6-diamidino-2-phenylindole (DAPI, Sigma Aldrich, Cat#ab228549) staining (1:10 000; 10 min, RT). Finally, cells were mounted onto slides using Mounting Media. Images were captured at 5-7 randomly selected fields of view using the same exposition time with a NIKON Eclipse Ti-E/80i fluorescent microscope (Nikon Instruments Inc., NY, USA). Pictures were analyzed using ImageJ software with cell counter plugin (National Institutes of Health, Bethesda, MD, USA). The number of nuclei showing characteristic apoptotic morphology (*i.e.,* condensation, micronuclei formation or fragmentation) were counted and expressed as percentage of total cell count.

3.6. Western blot analysis

Western blot analysis was performed to measure the expression and activation of proteins involved in the regulation and execution of apoptosis as well as of those contributing to mitochondrial quality control processes in cardiac cells subjected to SI/R with or without KYNA or Zaprinast treatment. Sample preparation and protein concentration measurement were performed as described previously [77]. Briefly, proteins were first separated in 10 % polyacrylamide gels, then blotted onto 0.45 µm pore-size polyvinylidene fluoride membranes (60 or 90 min, RT). Membranes were then cut horizontally according to the molecular weights of target proteins and incubated in 5% v/v BSA for 1 hour at RT (Serva, Cat#11920.06) to block unspecific binding. Incubation with specific primary antibodies against target proteins listed in *Table 1.* was performed then, followed by exposure to horseradish peroxidase-conjugated Goat Anti-Rabbit secondary antibody (DAKO, Agilent, Santa Clara, California, United States; Cat#P0048, 120 min, RT). LumiGlo reagent (Cell Signaling Technology, Cat#7003) was applied for 5 minutes at RT to enhance chemiluminescence, followed by the exposure of membranes to X-ray films. Finally, all films were scanned (8-bit, 400 dpi) and the density of each protein band was quantified using Quantity One software (Bio-Rad company, Hercules,

California, United States). Protein expression was normalized to the expression of corresponding housekeeping proteins. Caspase activities were expressed as cleaved/procaspase ratios.

Protein	Primary Manufacturer, Catalog No.	Conditions
BAX	CST, Cat#	1:1000, 4°C, on
Bcl-XL	CST, Cat#	1:1000, 4°C, on
Bcl-2	Abcam, Cat#	1:2000, 4°C, on
Caspase-3	CST, Cat#14220	1:1000, 4°C, on
Cleaved caspase-3	CST, Cat#9664	1:1000, 4°C, on
Caspase-7	CST, Cat#9492	1:1000, 4°C, on
Cleaved caspase-7	CST, Cat#9491	1:1000, 4°C, on
γ-H2AX	Abcam, Cat#	1:1000, 4°C, on
MFN2	CST, Cat#11925	1:1000, 4°C, on
OPA1	CST, Cat#80471	1:1000, 4°C, on
DRP1	CST, Cat#8570	1:1000, 4°C, on
α-tubulin	CST, Cat#2114	1:2000, 4°C, on
GAPDH	CST, Cat#2118	1:10000, 4°C, on

Table 1. **Primary antibodies used for western blotting.**

*(CST: Cell Signaling Technology, **BAX**: Bcl-associated X, **Bcl-XL**: B-cell lymphoma extra-large, **Bcl-2**: B-cell lymphoma 2, **γ-H2AX**: phosphorylated histone H2A variant X, **MFN2**: mitofusin-2; **OPA1**: optic atrophy 1; **DRP1**: dynamin-related protein 1, **GAPDH**: glyceraldehyde-3-phosphate dehydrogenase; **on**: overnight)*

3.7. Immunocytochemistry

Fluorescent microscopic analysis was applied to detect caspase-8 activity. For this, H9c2 cells were seeded onto glass coverslips at a density of 2×10^4 cells/well, and grown for two days. Cells subjected to SI/R were treated with 64 μM KYNA or its vehicle. A control group of cells was kept under normoxic conditions. At the end of the simulated reperfusion, cultures were fixed using 4% PFA (20 min, RT). Next, cells were permeabilized using 0.3% Triton X-100-containing PBS (20 min, RT), followed by blocking in 5% BSA-containing PBS (30 min, RT). Incubation with primary antibodies against procaspase-8 (Cell Signaling Technology, Cat#4790) and cleaved caspase-8 (Cell Signaling Technology, Cat#9748) was carried out next (1:150, overnight, 4 °C). For the period of primary incubations, cells were kept in a humidified chamber. Samples were then washed with PBS supplemented with 0.1% Tween-20, followed by incubation with Alexa-488/Alexa-647 fluorophore-conjugated Goat Anti-Rabbit or Goat Anti-Mouse secondary antibodies (1:300, 40 min, RT). Cell nuclei were stained with DAPI (1:10000, 10 min, RT). After a final washing step, coverslips were mounted onto slides using Mounting Medium, followed by visualization of cells with a Nikon Eclipse Ti-E microscope (Nikon Instruments Inc.,). Images were captured of at least 5 randomly selected fields of view

per sample using the same exposition time. Raw images were processed using Image J software by observers blinded to the experimental conditions. For fluorescence intensity measurement, images were first converted into 8-bit greyscale file format. Fluorescence intensity was then quantified by measuring mean grey value. Data were normalized to cell count. Images showing poor quality or imperfect staining were excluded from the evaluation.

3.8. Detection of caspase-3/-7 activity

To further confirm the potential KYNA-derived effects on the SI/R-induced alterations of proapoptotic signaling, H9c2 cells were subjected to SI/R with or without KYNA treatment, followed by caspase-3/7 activity measurement using Caspase-Glo 3/7 Assay (Promega, Madison, Wisconsin, USA; Cat#G8090) according to the manufacturer's instructions.

3.9. Electron microscopy

To prepare samples for electron microscopic calcium level assessment and mitochondrial morphometry, cardiac cells were collected from 75 cm^2 tissue culture flasks immediately after SI/R using 0.25% Trypsin-EDTA for 5 min at 37°C. Cells were then centrifuged (5 min, RT, 400 x g), and washed in PBS, followed by another centrifugation step (5 min, RT, 400 x g). Pellets were fixed using 3% glutaraldehyde (Polysciences Inc., Warrington, UK; Cat#111-30-8; pH was adjusted to 7.40 using KOH) supplemented with 90 mM of potassium oxalate (pH 7.40) (overnight, 4°C) and rinsed in 7.5% sucrose (Molar Chemicals Kft., Halásztelek, Hungary; Cat#02200) solution containing 90 mM potassium oxalate. Postfixation was performed via incubation in 2% potassium pyroantimonate (Merck, Burlington, Massachusetts, United States; Cat#12208-13-8) supplemented with 1% osmic acid (Sigma Aldrich, Cat#201030) for 2 hours at 4°C. Samples were then rinsed in distilled water for 10 min, followed by dehydration using an ascending series of ethanol (from 50% to 100%), and treatment with propylene oxide. Finally, samples were embedded in Durcupan ACM epoxy resin (Sigma Aldrich; Cat#44611) and polymerized for 48 hours at 56 °C. Semithin (0.5 μm) sections were prepared using an Ultracut UCT ultramicrotome (Leica Microsystems; Wetzlar, Germany). Ultrathin (50 nm) sections were then cut and mounted on single-hole copper grids (Electron Microscopy Sciences; Hatfield, PA, United States), contrasted with 2% uranyl acetate (Electron Microscopy Sciences) in 50% ethanol, and 2% lead citrate in distilled water. Ultrathin sections were examined in a JEM-1400Flash transmission electron microscope (JEOL; Tokyo, Japan). Sections were screened at low magnification (2–4000×) to locate 10–15 randomly selected cells. From each cell, images from randomly selected cytoplasmic regions were recorded as 16-bit grayscale images at 10000× magnification with a Matataki Flash (JEOL)

2k×2k high-sensitivity scientific complementary metal-oxide-semiconductor camera. As a result of the applied sample preparation method, electron-dense deposits (EDDs) were present due to the pyroantimonate-induced precipitation of intracellular calcium ions. The relative volume of mitochondrial EDDs was determined by point counting methods [78, 79]. Mitochondrial morphometry on electron microscopic images was performed using Image-Pro Plus software (Media Cybernetics; Rockville, MD, United States). Each mitochondrion (average of 40 mitochondria per sample) was segmented, and morphometric parameters such as average area of mitochondria, Feret's diameter, aspect ratio, circularity and perimeter were measured [80–82].

3.10. MitoTracking

To examine whether KYNA has an impact on the SI/R-induced alterations of mitochondrial architecture, cells were seeded onto glass coverslips at a density of $1.5x10^4$ cells/well, grown in 24-well plates for two days, and subjected to SI/R with or without 64 µM KYNA treatment. Normoxic samples were prepared as controls. MitoTracker Deep Red (Thermo Fisher Scientific, Waltham, Massachusetts, United States; Cat#M22426) was applied to label mitochondria of living H9c2 cells immediately after the SI/R protocol (1 µM, 30 min, 37°C), followed by fixation of cells using 4% PFA for 20 min at RT. Nuclei were labelled using Hoechst (1:4000, 10 min, RT). Coverslips were mounted onto slides using Mounting Medium, followed by visualization with a NIKON Eclipse Ti-E/80i fluorescent microscope (Nikon Instruments Inc.,) using the same exposition time for all samples. 6-9 randomly selected fields of view were captured per sample at 40X magnification. An observer blinded to the experimental conditions scored cells according to whether they exhibit aggregate-like structures along their mitochondrial network [83]. Cells exhibiting uncertain morphology as well as images showing imperfect staining were excluded from the analysis. The number of cells displaying impaired mitochondrial architecture was expressed as percentage of total cell count and compared to the corresponding control groups.

3.11. RNA isolation and quantitative polymerase chain reaction (qPCR)

To investigate the expression of genes encoding proteins governing mitochondrial quality control mechanisms (*i.e.,* fusion and fission), total RNA was isolated from H9c2 cells grown in 75 cm^2 tissue culture flasks undergoing SI/R with or without KYNA treatment using a Monarch® Total RNA Miniprep Kit according to the manufacturer's instructions (New England BioLabs, Ipswich, Massa-chusetts, United States; Cat#T2010S). RNA was then transcribed into cDNA using Maxima First Strand cDNA Synthesis Kit for RT-qPCR (Thermo Fisher Scientific;

Cat#K1642). Luminaris Color HiGreen Low ROX qPCR Master Mix (Thermo Fisher Scientific; Cat#K0373) was used next to perform RT-PCR. Sample amplification was performed under the following conditions: 10 min at 95 °C, then 40 cycles of 95 °C for 15 sec and 60 °C for 1 min. Relative transcript levels were measured using 18S rRNA as reference gene. The applied primers are listed in *Table 2*.

Genes	Forward primers	Reverse primers
Mfn1	GAAGGCCTGTCCAGAACTGA	CCGGGTTCCTGTATGTTGCT
Mfn2	CCCTTACCAGCTAGAAACGAGA	GACAAAGTGCTTGAGAGGGGA
Opa1	TGCTGTTGGAGGTGGCTATAC	GGTGTACCCGCAGTGAAGAA
Drp1	CGTAGTGGGAACTCAGAGCAG	ACCCCATTCTTCTGCTTCAACT
Fis1	GGTTGCGTGGTAAGGGATGA	CAAACTGCGTGCTCTTGGAC
Gpr35	GCTCTTTGCAGGTTGTGACTG	GCACGGCTGAAGATGTTTCG

Table 2. **Primers used for RT-PCR.**

***Mfn1**: mitofusin-1; **Mfn2**: mitofusin-2; **Opa1**: optic atrophy 1; **Drp1**: dynamin-related protein 1; **Fis1**: mitochondrial fission protein 1, **Gpr35**: G-protein coupled receptor 35*

3.12. Measurement of mitochondrial superoxide production

MitoSOX Mitochondrial Superoxide Indicator (Thermo Fisher Scientific; Cat#M36008) was applied to assess the mitochondrial damage associated oxidative stress. H9c2 cells seeded at a density of 1.5 x 10^4 cells/well into 24-well plates containing glass coverslips were subjected to SI/R with or without 64 μM KYNA treatment, followed by incubation under 2.5 μM MitoSOX-containing DMEM for 15 minutes at 37°C. Live cell imaging was performed using a Nikon Eclipse Ti-E microscope (Nikon Instruments Inc.). Photos were captured at 6-9 randomly selected fields of view using the same exposition time for all samples. Image J software was applied to carry out image analysis, which was performed by an observer blinded to the experimental conditions. Images were converted to 8-bit format, followed by the measurement of mean grey value to assess fluorescence intensity in 10 randomly selected cells per view field.

3.13. Estimation of mitochondrial membrane potential using JC-1 staining

To determine if KYNA administration improves the SI/R-induced alterations in mitochondrial membrane potential, JC-1 staining was performed on living H9c2 cells [77]. For this, at the end of simulated reperfusion, cells were washed and incubated with DMEM supplemented with 10 μg/mL JC-1 dye (Thermo Fisher Scientific, Cat#M34152) for 10 min at 37°C. Cells were then washed and covered with 10% v/v FBS-containing DMEM. JC-1-stained cells were visualized by an OLYMPUS BX51 (Olympus corporation, Shinjuku, Tokyo, Japan)

microscope equipped with Olympus DP70 camera using the same exposition time for all samples. Red/green fluorescent ratio representing mitochondrial membrane potential was determined using Image J software.

3.14. High-Resolution Respirometry

Mitochondrial O_2 consumption was assessed in H9c2 cells using High-Resolution FluoRespirometry (Oxygraph-2k, Oroboros Instruments, Innsbruck, Austria). At the end of SI/R, cells were collected using 0.25% Trypsin-EDTA (5 min, 37°C). $3x10^6$ cells were then centrifuged (5 min, RT, 400 x g), washed in PBS, resuspended in 2.3 mL Mir05 medium and gently pipetted into the respiration chamber. When a stable baseline respiration has been reached (ROUTINE respiration without external substrates), cells were permeabilized with digitonin (20 µg/mL) (*Figure 7*). Complex I-dependent oxidative phosphorylation capacity (OXPHOS I) was measured in the presence of complex I-linked substrates (10 mM glutamate and 2 mM malate) and ADP (2.5 mM) [33]. Rotenone was used at a concentration of 0.5 µM to inhibit Complex I and separate Complex II-dependent oxidative phosphorylation capacity (OXPHOS II) in the presence of 10 mM succinate and adenylate (*Figure 7*). After antimycin A-induced inhibition of complex III, the respiratory activity of Complex IV was measured in presence of ascorbate (2 mM) and artificial substrate TMPD (0.5 mM). Ascorbate was applied before TMPD to avoid uncontrollable autoxidation of the electron donor. Sodium azide (NaN3; 100 mM) was supplemented finally, to block Complex IV-linked mitochondrial O_2 consumption (*Figure 7*) [84]. All the measurements were performed during continuous stirring at 37 °C. DatLab software (Oroboros Instruments) was used for online display, respirometry data acquisition and analysis. Respiratory substrates and inhibitors were purchased from Sigma Aldrich. Data were illustrated as O_2 flow per cells and expressed in pmol/(s∗million cells).

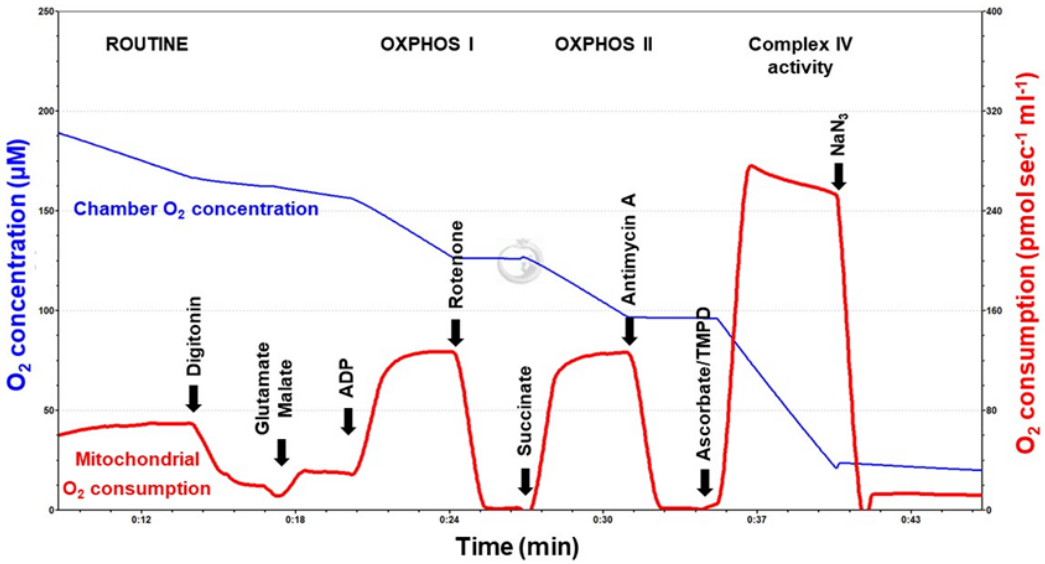

Figure 7. **Respirometry protocol.**

***ADP**: adenosine diphosphate, **OXPHOS I**: complex-I-dependent oxidative phosphorylation capacity, **OXPHOS II**: complex-II-linked oxidative phosphorylation capacity*

3.15. Measurement of cell viability

3.15.1. Calcein assay

Calcein staining was applied to determine cell viability after SI/R according to a previously published protocol [77]. Briefly, after washing cells with warm Dulbecco's Phosphate Buffer Solution (D-PBS; Sigma Aldrich, Cat#D8537), cells were covered with D-PBS containing 0.5 µM Calcein-AM (Thermo Fisher Scientific, Cat#C3100MP) and placed into a standard CO_2 incubator for 30 minutes. After the incubation, Calcein dye was replaced with D-PBS, and fluorescence intensity was measured at 490 nm excitation and 510 nm emission wavelengths using a microplate reader (BMG ClarioStar Plus/Fluostar Optima, BMG Labtech, Ortenberg, Germany). Viability was expressed as percentage of average viability detected in the corresponding control groups.

3.15.2. MTT assay

To assess viability in experiments studying the effect of KYNA on camptothecin-induced apoptotic cell death of cardiac cells, 3-(4,5-dimethylthiazol-2-yl)-2,5-diphenyltetrazolium bromide (MTT; Sigma Aldrich, Cat#M2128) assay was applied. At the end of the protocol, treatment solutions were removed gently and replaced with 1% v/v FBS-containing DMEM supplemented with 0.5 mg/ml MTT for 1 hour (37°C, standard CO_2 incubator). DMSO was then used to dissolve formazan crystals, followed by the measurement of absorbance at 590 nm using a microplate reader (BMG ClarioStar Plus/Fluostar Optima). Viability was expressed as percentage of the average viability observed in the corresponding control groups.

3.16. Statistical analysis

Statistical analysis was carried out using Prism 8.0 software (GraphPad Software, GraphPad Software Ldt., Cali-fornia, United States). Graphs represent data expressed as mean ± standard error of the mean (SEM). During the analysis, normality of sample distribution was assessed first, using Shapiro-Wilks normality test in each case. In case of normal data distribution, comparisons involving more than two groups were assessed using one-way ANOVA. *Post hoc* analysis was performed with either Fisher' LSD test (*i.e.,* when the sample size was less than 10) or Tukey's multiple comparisons test (*i.e.,* when the sample size exceeded 10). In case of non-normal distribution, data sets were analyzed using Kruskal-Wallis test with Dunn's multiple comparisons test as *post hoc* analysis.

4. Results

4.1. KYNA treatment decreased the number of cells showing apoptotic morphology

Morphological hallmarks of apoptosis, including apoptotic membrane blebbing and characteristic nuclear morphology were observed first, to investigate the effects of KYNA on apoptosis in the setting of SI/R. When investigating membrane blebbing, the percentage of cells showing healthy or slightly altered membrane morphology decreased substantially upon exposure to SI/R, while the ratio of those showing signs of propagating apoptosis increased significantly compared to the corresponding normoxic controls (*Figure 8A*). However, KYNA treatment was found to maintain the ratio of healthy cells, as well as to decrease the percentage of those exhibiting morphological hallmarks of progressing apoptosis (*Figure 8A*). Assessment of nuclear morphology revealed that SI/R caused a significant elevation in the percentage of cells showing apoptotic nuclear morphology (*Figure 8B-C*), which increase diminished upon KYNA treatment (*Figure 8B-C*).

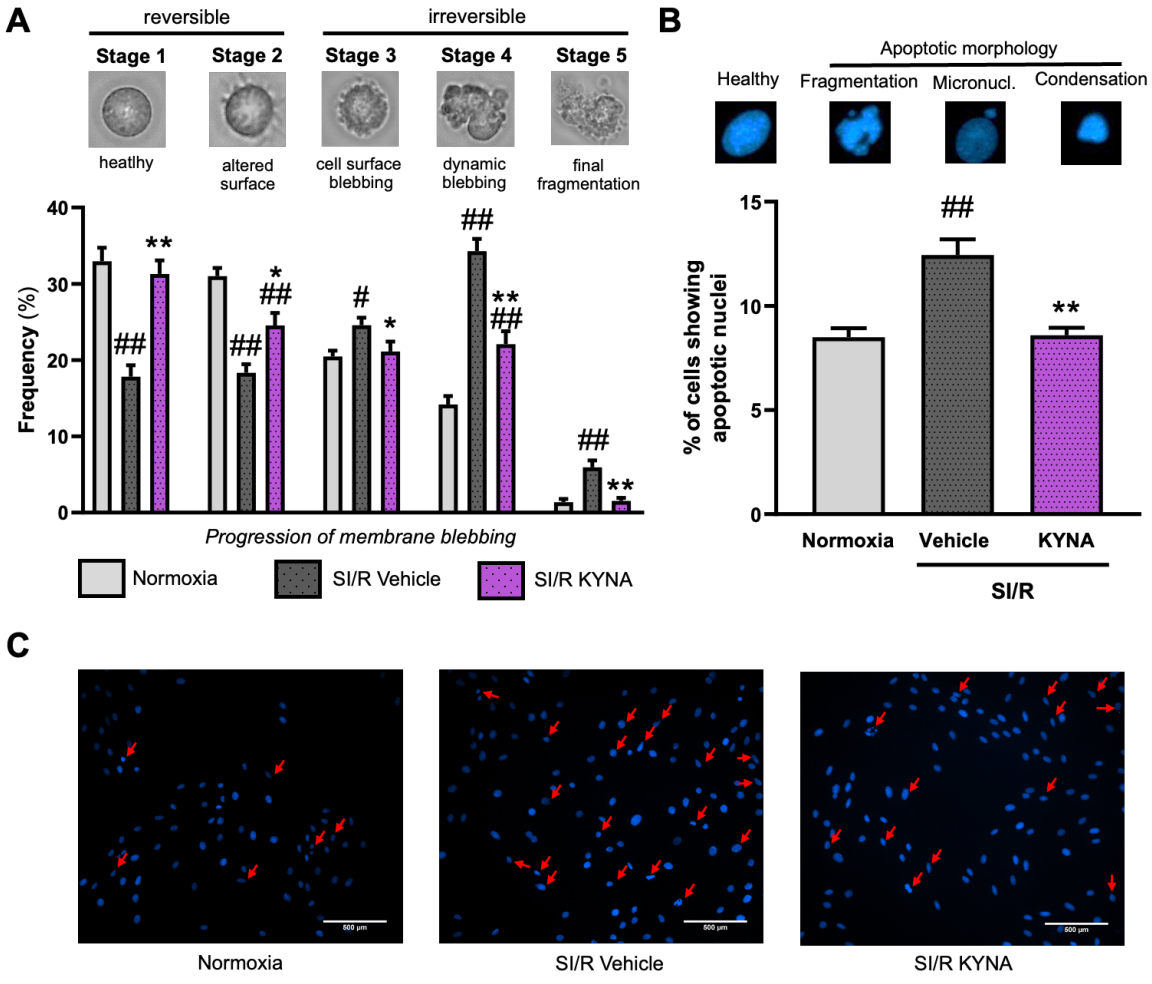

Figure 8. **The effects of KYNA on apoptotic morphology in cells undergoing SI/R.**

*(**A**) Membrane blebbing assessed in n = 3–4 samples/experiment, 6–10 randomly selected fields of view/sample, 3 separated experiments (average % of cells scored into the presented stages of membrane blebbing ± SEM, #p<0.05, ##p<0.01, *p<0.05 **p<0.01, Kruskal-Wallis test with Dunn's multiple comparisons test). (**B-C**) Nuclear morphology in n=2-4 samples/experiment, 5-6 randomly selected fields of view/sample, 2 independent experiments with representative images. Red arrows indicate nuclei showing apoptotic signs (average % of cell nuclei showing apoptotic morphology ± SEM, ##p<0.0001, **p=0.0007, Kruskal-Wallis test with Dunn's multiple comparisons test).*

4.2. KYNA seemed to prevent the SI/R-induced shift towards proapoptotic signaling

To investigate the molecular events laying behind the KYNA-derived protection against SI/R-induced cardiac cell damage, protein expression of various mediators involved in either the initiation or execution of apoptosis was measured via western blotting. Assessment of apoptosis regulatory proteins revealed that SI/R increased the level of proapoptotic BAX significantly (*Figure 9A*), while exerting no substantial effects on the expression of antiapoptotic Bcl-XL (*Figure 9B*) or Bcl-2 (*Figure 9C*). Importantly, KYNA administration was found to reduce the SI/R-enhanced BAX expression considerably, keeping it close to that observed in the corresponding normoxic control group (*Figure 9A*). Furthermore, KYNA administration increased the level of protective Bcl-XL substantially in cells undergoing SI/R (*Figure 9B*). In case of Bcl-2, no significant KYNA-driven effects were observed (*Figure 9C*).

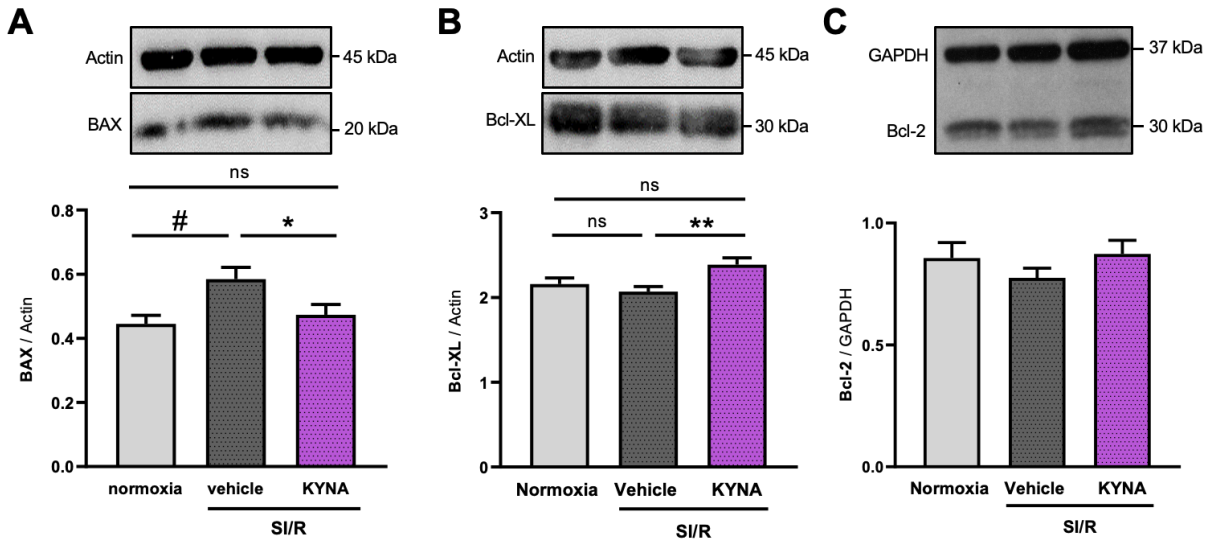

Figure 9. **KYNA administration seemed to prevent the SI/R-induced shift towards proapoptotic signaling through altering the expression of apoptosis modulatory proteins.**

*Representative pictures and relative protein expression of (**A**) proapoptotic BAX, antiapoptotic (**B**) Bcl-XL and (**C**) Bcl-2 apoptosis modulatory proteins in n=3-5 samples/experiment, from 2-3 independent experiments (average protein expression relative to housekeeping controls ± SEM, #p=0.011; *p=0.0495, **p=0.0075; ANOVA with Tukey's multiple comparisons test).*

4.3. KYNA was found to suppress extrinsic apoptotic mechanisms

Next, we assessed whether KYNA administration suppresses the SI/R-induced activation of extrinsic apoptotic mechanisms. For this, extrinsic initiator caspase-8 levels were assessed via fluorescent microscopy. Here we have found that procaspase-8 levels were not affected by SI/R substantially; however, KYNA seemed to reduce its baseline expression substantially, compared to that found in vehicle-treated cells subjected to SI/R (*Figure 10B-C*). Cleaved caspase-8 expression assessments revealed that capsase-8 activation increased considerably upon exposure to SI/R (*Figure 10B, D*). However, KYNA treatment was found to reduce the degree of the SI/R-induced extrinsic apoptosis initiation, as revealed by considerably lower cleaved caspase-8 levels (*Figure 10B, D*).

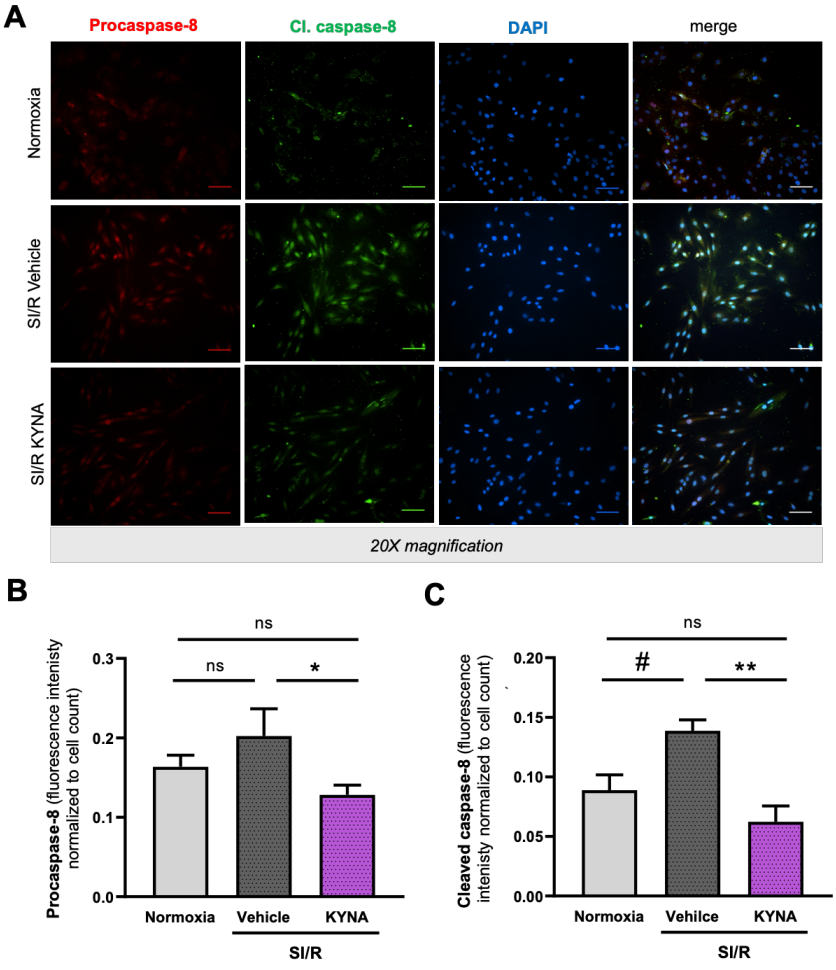

Figure 10. **KYNA treatment suppressed the SI/R-induced extrinsic apoptotic initiation.**

*(**A**) Representative pictures of fluorescence microscopy, taken at 20X magnification. Scale bar: 500 µm. Relative (**B**) procaspase-8 and (**C**) cleaved caspase-8 expressions in n = 2 samples, 5-6 images taken from randomly selected fields of view/samples, from 2 independent experiments (average expression normalized to cell count ± SEM, procaspase-8: *p=0.042; one-way ANOVA with Dunnett's multiple comparisons test, cleaved caspase-8: average expression normalized to cell count ± SEM, *p=0.042; one-way ANOVA with Dunnett's multiple comparisons test).*

4.4.The execution of apoptosis was attenuated by KYNA

The activity of executioner caspases was measured next to confirm the involvement of apoptosis in the SI/R-triggered cardiac cell damage in our model, as well as to further examine the potential antiapoptotic effects of KYNA. Western blotting revealed that SI/R caused a substantial increase in the activation of both caspase-3 (*Figure 11A*) and caspase-7 proteins (*Figure 11B*). KYNA treatment, on the other hand, was found to reduce cleaved/procaspase-3 ratio significantly (*Figure 11A*). In case of caspase-7, KYNA was shown to prevent the SI/R-induced considerable increase in cleaved to procaspase-7 ratio, maintaining caspase-7 activity closer to that found in the normoxic control group (*Figure 11B*). To corroborate these KYNA-derived effect on caspase activities, luminescence-based caspase-3/-7 activity test was performed, revealing that the SI/R-induced activation of caspases was ameliorated upon KYNA treatment (*Figure 11C*). Relative phosphorylated histone H2A variant (γ-H2AX) expression, indicative of the degree of DNA double-strand break damage was quantified then. Here, SI/R was shown to increase the expression of γ-H2AX significantly, which effect was attenuated by KYNA administration considerably (*Figure 11D*).

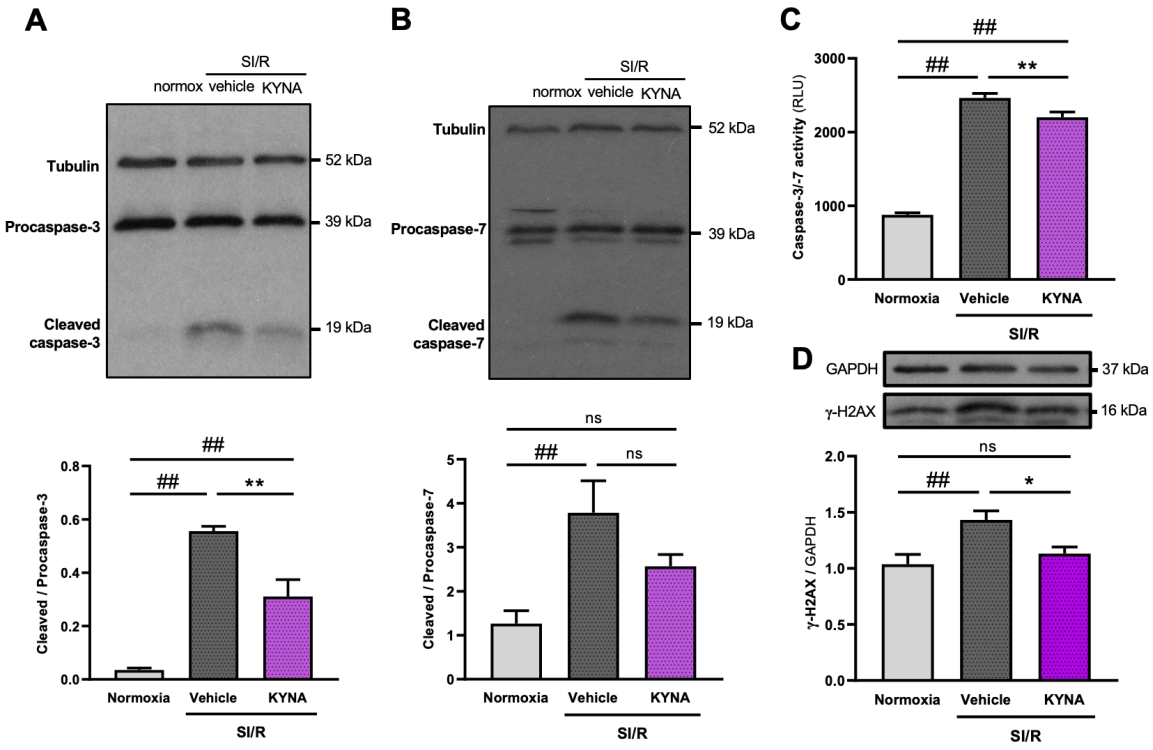

Figure 11. **KYNA administration reduced the SI/R-induced activation of apoptosis executionary proteins.**

*Representative pictures and protein expression of (**A**) cleaved caspse-3 and (**B**) cleaved caspase-7 normalized to procaspase-3 and procaspase-7, respectively, in n=3-4 samples/experiment, from 2 independent experiments (average cleaved to procaspase ratios ± SEM, ##p<0.01 and **p<0.01,*

*ANOVA with Tukey's multiple comparisons test). (**C**) Caspase-3/-7 activity measurement in n=11-15 samples/experiment, from 3 separate experiments (average relative luminescence ± SEM, ##p<0.0001; **p=0.0057; one-way ANOVA with Tukey's multiple comparisons test). (**D**) γ-H2AX expression relative to housekeeping control in n=3 samples/experiment, 2 independent experiments (relative protein expression ± SEM, ##p=0.006 and *p=0.036, ANOVA with Tukey's multiple comparisons test).*

4.5. KYNA administration rescued cardiac cells exposed to camptothecin treatment

In order to confirm its antiapoptotic effects, KYNA was tested in a separate experimental model in presence of a well-known apoptosis inducer, camptothecin (*Figure 12A*) [85]. Here we have found that camptothecin exposure decreased cell viability substantially compared to that observed in untreated controls (*Figure 12B*). KYNA treatment, however, improved the survival compared to vehicle-treated cells subjected to camptothecin (*Figure 12B*).

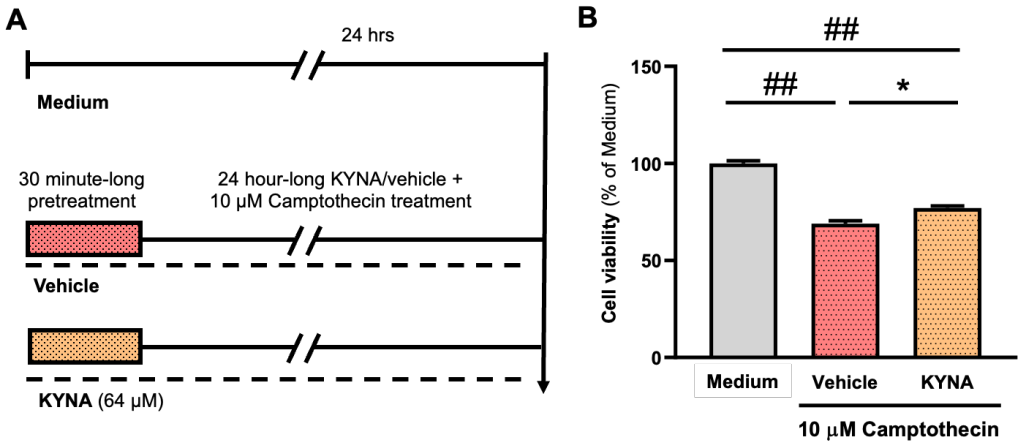

Figure 12. **KYNA treatment rescued cardiac cells undergoing treatment with camptothecin.**

*(**A**) Experimental protocol. (**B**) Effects of KYNA against the Camptothecin-induced decrease in cell viability in n=14 samples per experiment, from 4 independent experiments (average % of cell viability ± SEM, ##p<0.001; *p=0.024; Kruskal-Wallis test with Dunn's multiple comparisons test).*

4.6. KYNA treatment prevented the intramitochondrial calcium buildup and maintained mitochondrial ultrastructure in cells exposed to SI/R

As Ca^{2+} overload is considered to be a fundamental contributor to SI/R-injury as well as a signal to initiate apoptosis, next we assessed the effects of KYNA on intramitochondrial Ca^{2+} levels via electron microscopy. Here, SI/R was found to cause a substantial intramitochondrial Ca^{2+} buildup, which effect seemed to diminish when KYNA was administered throughout SI/R (*Figure 13A-B*). Keeping that in mind increased Ca^{2+} levels are known to induce mechanisms damaging mitochondrial structure and function [86], next we assessed various morphological parameters (*i.e.*, aspect ratio, mitochondrial Feret's diameter, perimeter, average area of

mitochondria and circularity) on electron microscopic images. Among these, aspect ratio (*Figure 13C*), Feret's diameter (*Figure 13D*), perimeter (*Figure 13E*) and average area of mitochondria (*Figure 13F*) were shown to increase significantly upon SI/R, while circularity decreased considerably in cells exposed to SI/R (*Figure 13G*). KYNA administration, however, was found to diminish these SI/R-triggered alterations. Cells treated with KYNA exhibited significantly decreased aspect ratio (*Figure 13C*), furthermore, KYNA was shown to maintain levels of Feret's diameter (*Figure 13D*), perimeter (*Figure 13E*), and average area (*Figure 13F*) closer to that found in normoxic controls, preventing their significant SI/R-induced elevation. Additionally, KYNA administration seemed to prevent the SI/R-induced alterations in circularity (*Figure 13G*).

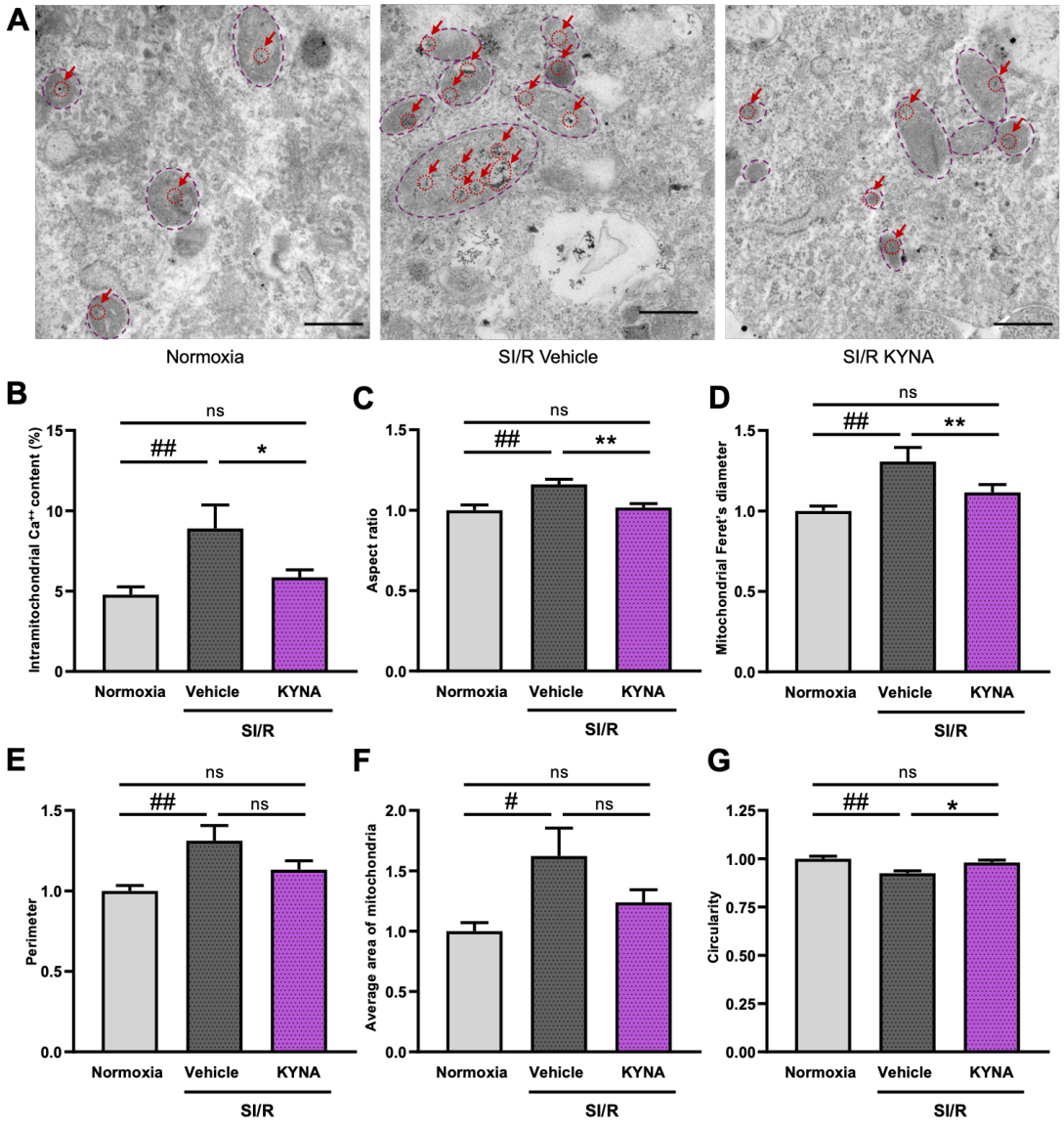

Figure 13. **KYNA treatment ameliorated the SI/R-induced intramitochondrial calcium buildup as well as the alterations in mitochondrial ultrastructure.**

*(**A**) Representative images of electron microscopy, Red arrows indicate calcium precipitates. Dashed lines outline mitochondria. (**B**) Intramitochondrial calcium levels in n=2 samples/experiment, 3 independent experiments (average intramitochondrial calcium levels ± SEM, ##p=0.0068; *p=0.035; one-way ANOVA with Fisher's LSD post hoc test). (**C**) Aspect ratio, (D) Mitochondrial Feret's diameter, (**E**) perimeter, (**F**) average area of mitochondria and (**G**) circularity in n=2-3 samples/experiment, 4 separate investigations (mean ± SEM, #p<0.05 and ##p<0.01; *p<0.05 and **p<0.01; one-way ANOVA with Tukey's post hoc test).*

4.7. KYNA decreased the ratio of cells exhibiting mitochondrial aggregates

To further investigate the effects of KYNA on the SI/R-induced alterations in the organization of mitochondria, MitoTracking was performed on cells undergoing SI/R with or without KYNA. SI/R was shown to increase the ratio of cells exhibiting aggregate-like structures in their mitochondrial network (*Figure 14A-B*). However, the substantial effect of SI/R on mitochondrial architecture seemed to diminish upon KYNA treatment (*Figure 14A-B*).

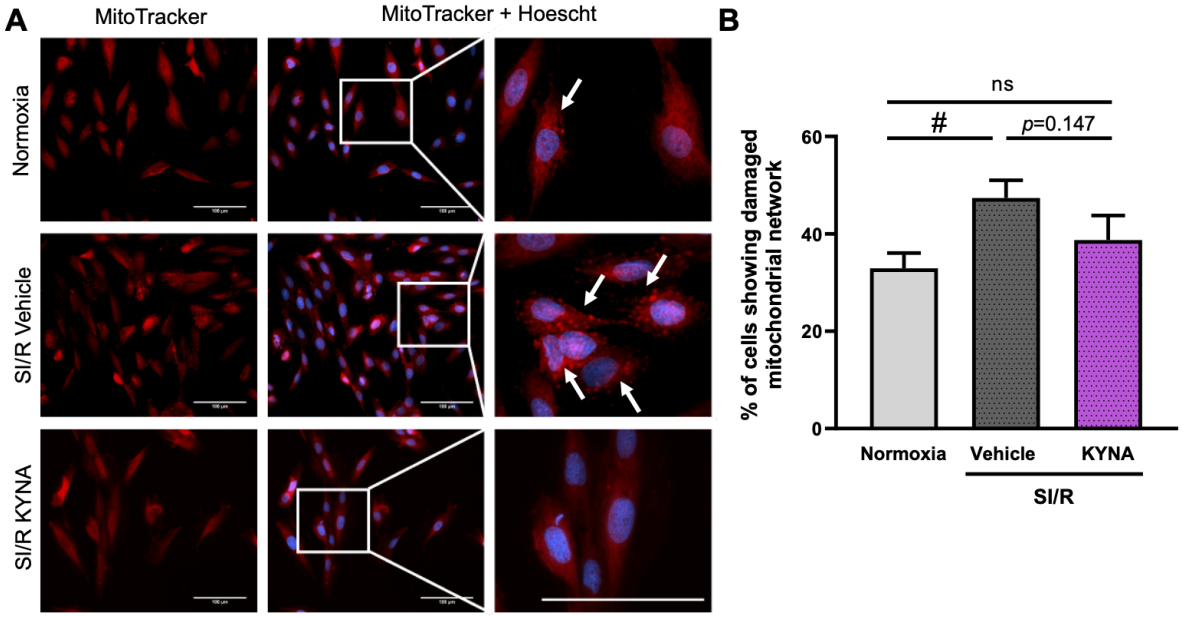

Figure 14. **KYNA treatment prevented the SI/R-induced aggregation of mitochondria.**

*(**A**) Representative pictures. White arrows indicate cells showing aggregate-like staining pattern. Scale bar: 100 µm. (**B**) Percentage of cells exhibiting aggregate-like morphology in n=1-2 samples/experiment from 4 independent investigations with 6-8 fields of view/sample analyzed (average % ± SEM, #p=0.0176; one-way ANOVA with Fisher's LSD post hoc test).*

4.8. The KYNA-triggered improvements in mitochondrial morphology seemed to occur independently of altered mitochondrial quality control mechanisms

As the results of both electron and fluorescent microscopy investigations suggested that SI/R as well as KYNA treatment seems to affect the structure and organization of the mitochondrial network, next we performed molecular analyses to examine whether altered

mitochondrial quality control mechanisms lay behind the observed morphological changes. The potential alterations in the expression of fusion- and fission-driving genes were measured through the detection of relative mRNA levels via RT-PCR. Here, SI/R was shown to stimulate the transcription of fusion-triggering genes, such as *Mfn1*, *Mfn2* and *Opa1*, significantly (*Figure 15A-C*). KYNA treatment, on the other hand, was found to either significantly reduce (*i.e.,* in case of *Mfn2*) or prevent (*i.e.,* in case of *Mfn1* and *Opa1*) the SI/R-aggravated transcription of profusion genes (*Figure 15A-C*). Assessments on the activity of fission-driving genes revealed that the transcription of both *Fis1* and *Drp1* genes increased substantially upon SI/R (*Figure 15D-E*). KYNA treatment, however, was shown to reduce the SI/R-induced upregulation of both investigated genes, significantly suppressing *Fis1* and *Drp1* mRNA levels compared to that found in vehicle-treated controls (*Figure 15D-E*). To confirm the SI/R- and KYNA-induced alterations in the molecular mechanisms driving fusion and fission, we measured the expression of MFN2, OPA1 and DRP1 proteins via western blotting (*Figure 15F-I*). Interestingly, western blotting revealed no significant SI/R- or KYNA-induced changes in neither of the investigated proteins' expression (*Figure 15F-I*).

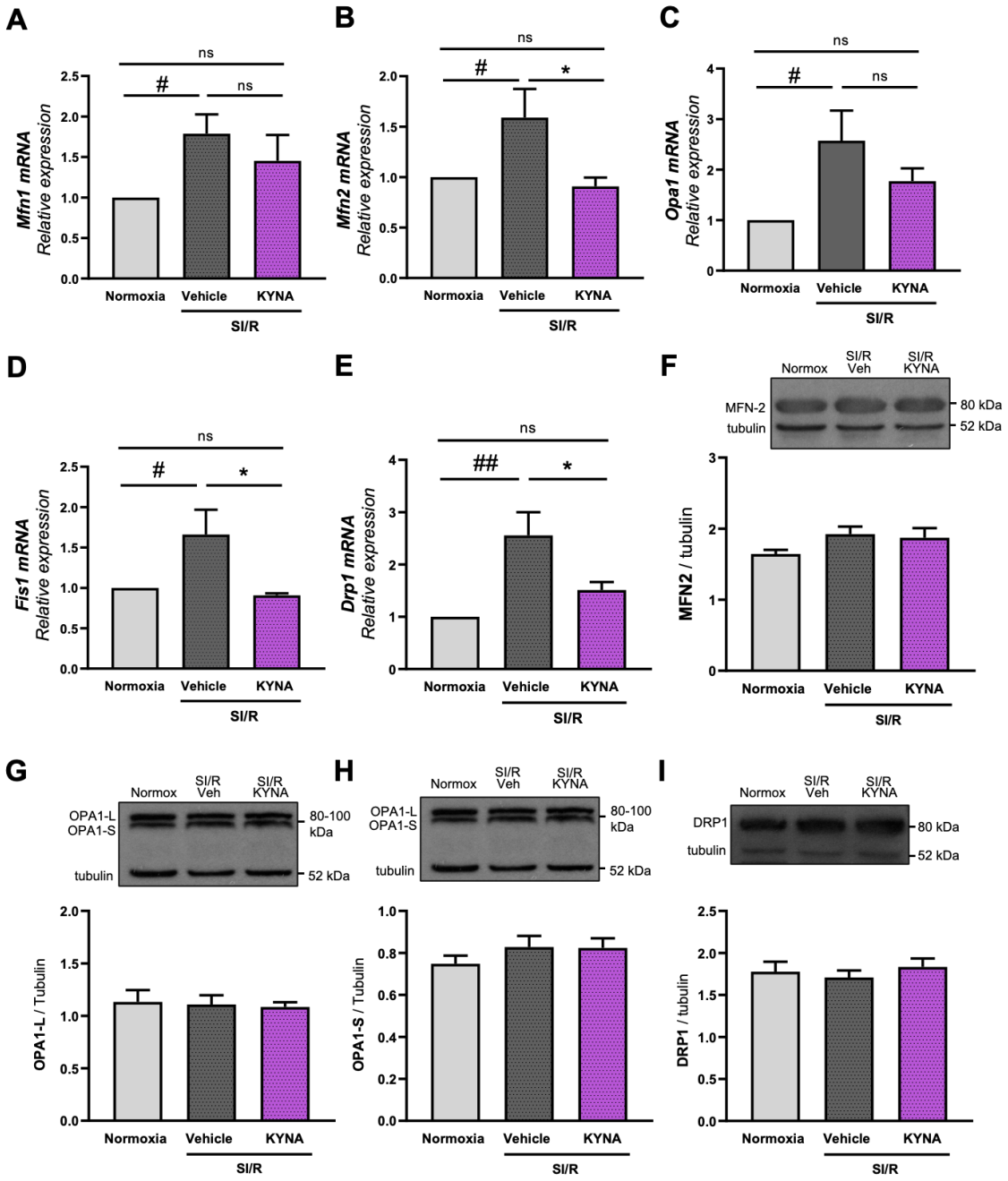

Figure 15. **KYNA treatment seemed to affect the activity of fusion- and fission-diving genes without influencing protein-level expressions.**

*Relative mRNA expression of (**A**) Mfn1, (**B**) Mfn2, (**C**) Opa1, (**E**) Drp1 and (**F**) Fis1 genes in n=7-8 samples/group from 3 independent experiments (mRNA expression relative to controls ± SEM, ##p<0.01 and #p<0.05 vs. Normoxia, *p<0.05 vs. SI/R+Vehicle, One-Way ANOVA with Fisher's LSD post hoc test). Expression of fusion and fission driving proteins (**F**) MFN2, (**G-H**) OPA-1/-2 and (**I**) DRP1 in n=9-13 samples/group, with samples being collected from 3-4 independent experiments (protein expression relative to housekeeping controls ± SEM, One-Way ANOVA with Tukey's multiple comparisons test).*

4.9. KYNA suppressed mitochondrial ROS release and loss of membrane potential

The I/R-induced impairment of mitochondria is known to increase the rate of mitochondrial ROS production, aggravating oxidative stress that contributes to and determines the development and extent of I/R-induced myocardial damage [87]. Hence, MitoSOX staining was performed to reveal the potential effects of KYNA against SI/R-induced mitochondrial ROS production. Here we have shown that cardiac cells undergoing SI/R exhibit significantly increased mitochondrial superoxide levels compared that found in case of corresponding normoxic controls (*Figure 16A-B*). However, cells receiving KYNA treatment maintained mitochondrial ROS levels close to that observe in normoxic cells despite exposure to SI/R (*Figure 16A-B*). Alterations of mitochondrial membrane potential were examined as well, revealing that the SI/R-induced depolarization of mitochondrial membranes diminished in cardiac cell cultures treated with KYNA (*Figure 16C-D*).

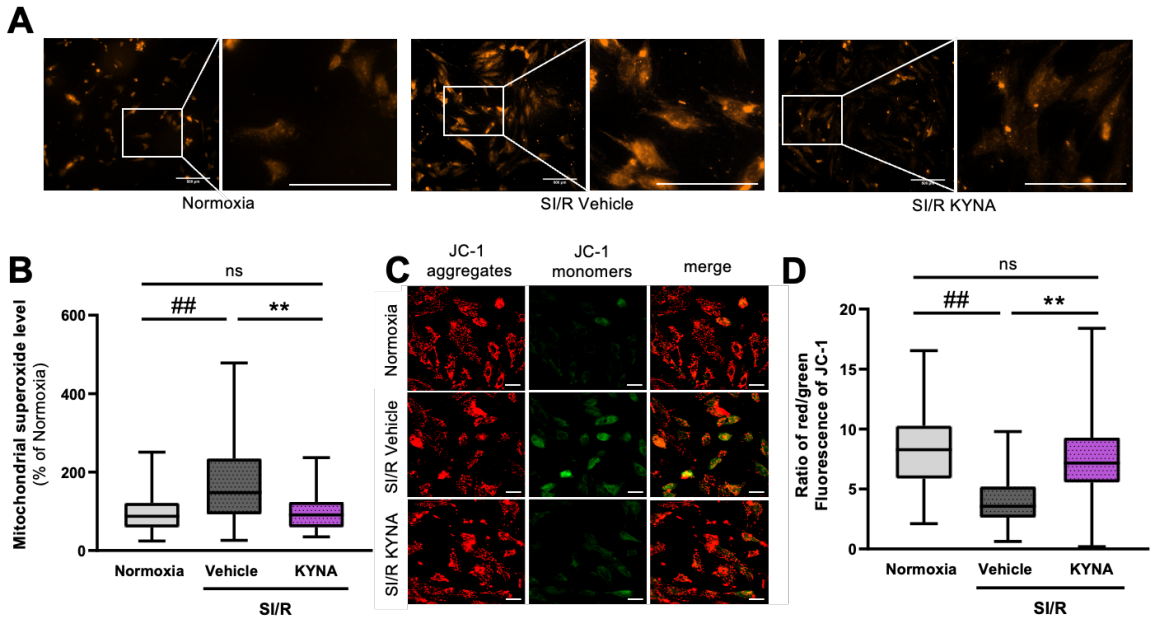

Figure 16. **Treatment with KYNA reduced the effects of SI/R on mitochondrial ROS-production and membrane depolarization.**

*(**A**) Representative pictures obtained after MitoSOX staining. Scale bar: 500 μm. (**B**) Mitochondrial superoxide levels in n=2-3 samples/experiment, 4 separated experiments (average % of normoxia ± SEM, ##p<0.0001 and **p<0.0001; Kruskal-Wallis test with Dunn's post hoc test). (**C**) Representative images of membrane potential measurements. Scale bar: 500 μm. (**D**) Average ratio of red/green fluorescence of JC-1 reflective of mitochondrial membrane potential in n=2 samples/experiment, 3 independent experiments (average red/green ratio ± SEM, ##p<0.0001 and **p<0.0001; Kruskal-Wallis test with Dunn's post hoc test).*

4.10. KYNA treatment preserved mitochondrial respiration in cells undergoing SI/R

To assess the functionality of mitochondria further, various respiratory parameters were measured using high-resolution respirometry in H9c2 cells undergoing SI/R with or without KYNA treatment. We have shown that baseline oxygen consumption of cardiomyoblasts decreased significantly upon exposure to SI/R (*Figure 17A*). Similar SI/R-induced deteriorating effects were observed in case of complex-I, -II and -IV-dependent oxidative phosphorylation (*Figure 17B-D*). KYNA treatment, however, was found to prevent such alterations, maintaining baseline oxygen consumption close to that observed in normoxic cultures (*Figure 17A*), as well as preserving respiratory functions in all the examined respiratory states (*Figure 17B-D*).

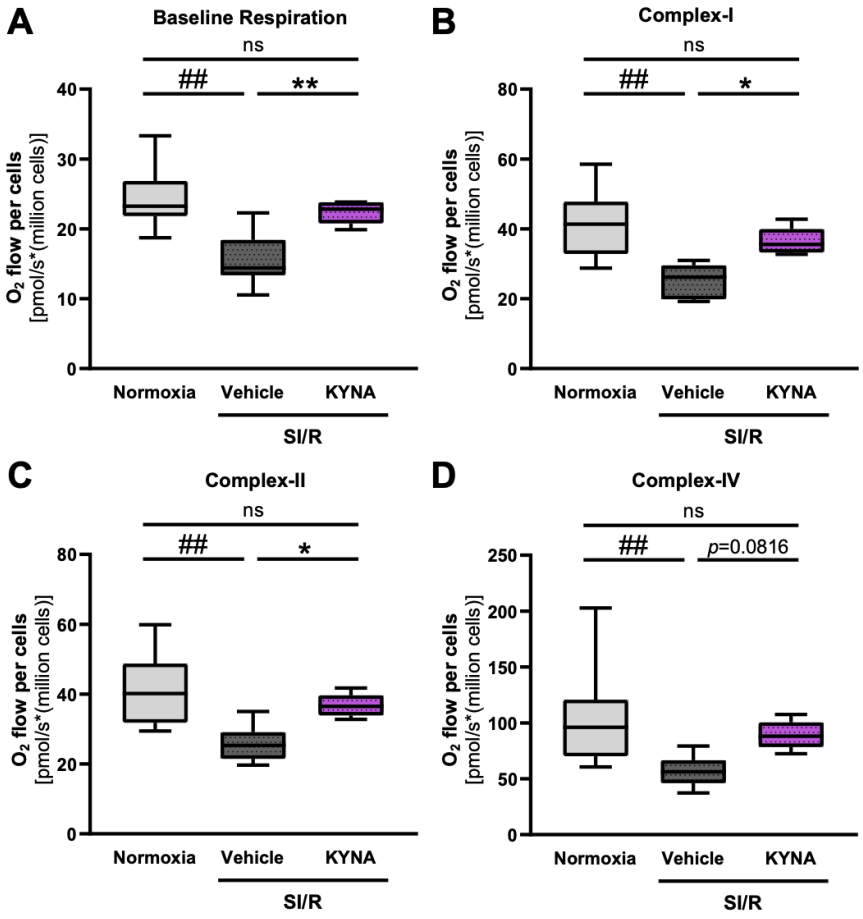

Figure 17. **KYNA treatment improved mitochondrial respiration in cells exposed to SI/R.**

*(**A**) Baseline respiration, (**B**) Complex-I dependent OXPHOS, (**C**) Complex-II dependent OXPHOS and (**D**) Complex-IV dependent OXPHOS in n=5-8 from 6 separate experiments (average O2 flow per cell ± SEM, ##p<0.01, **p<0.01 and *p<0.05, ANOVA with Fischer's LSD multiple comparisons test).*

4.11. GPR35 receptors are expressed by H9c2 cardiomyoblasts

Next, we aimed to investigate potential receptor-mediated mechanisms laying behind the KYNA-derived cardiocytoprotection. Along these examinations, we focused on the potential

involvement of GPR35 agonism in the protective effect of KYNA. First, to confirm the expression of GPR35 receptors on H9c2 cells, we detected relative *Gpr35* mRNA levels via quantitative RT-PCR. Our findings revealed that the receptors at our interest are present on H9c2 cardiomyoblasts (*Figure 18A-B*). Interestingly, KYNA administration seemed to stimulate the expression of GPR35 receptors further when compared to both control cultures (*i.e.,* cells maintained under media) and Normoxia+Vehicle groups (*Figure 18A-B*).

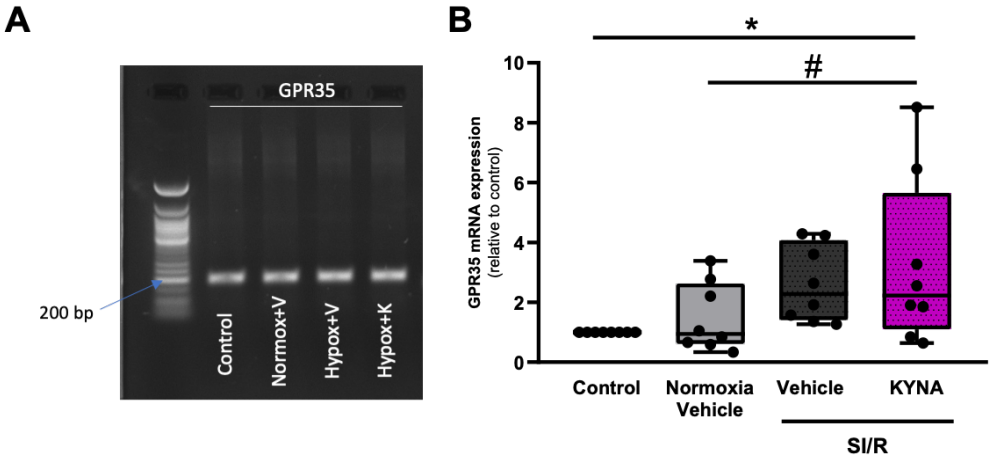

Figure 18. **GPR35 receptors are expressed by H9c2 cells.**

*(**A**) Representative picture. (**B**) GPR35 mRNA expression in n= 2-3 samples/experiment, 3 separated experiments (mRNA expression relative to control ± SEM, #p=0.039 and *p=0.0104, one-way ANOVA with Fischer's LSD post hoc test).*

4.12. GPR35 receptor agonism seemed to play a fundamental role in the cytoprotective effect of KYNA

Next, we aimed to assess whether the activation of GPR35 receptors plays a significant role in the KYNA-derived protection of cardiac cells exposed to SI/R. For this, cells were treated with either KYNA, CID2745687, a synthetic GPR35 receptor antagonist, or their combination throughout SI/R (*Figure 19A*). Similarly to our previous observations, SI/R decreased the survival of H9c2 cells substantially (*Figure 19B*). KYNA treatment, applied in the previously uncovered protective dose of 64 µM, however, improved cell viability substantially (*Figure 19B*). GPR35 receptor antagonism through CID2745687 administration had no significant effect on cell viability compared to SI/R+Vehicle controls (*Figure 19B*). Importantly, although KYNA treatment alone was found to rescue cells undergoing SI/R, when administered in parallel with CID2745687, achieving GPR35 antagonism, the KYNA-derived protective effects diminished (*Figure 19B*).

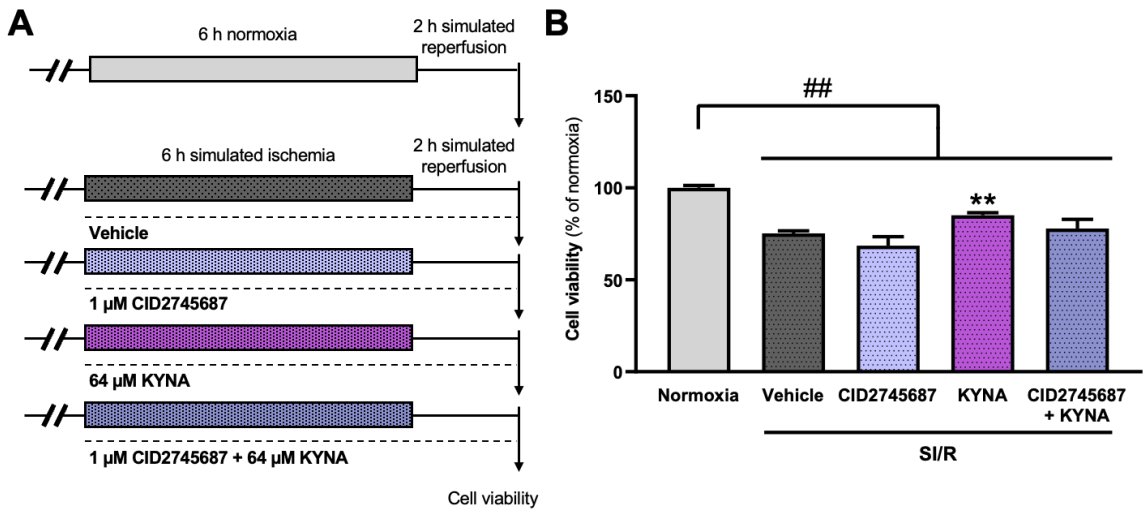

Figure 19. **The KYNA-induced cardiocytoprotection seemed to rely on GPR35 agonism.**

*(**A**) Experimental protocol of analyses aiming to uncover whether the GPR35 receptor activator feature of KYNA is necessary for its cardioprotective effect. (**B**) Cell viability in n=7-28 samples/experiment, with 4 independent experiments carried out (% of average viability detected in the normoxic control group ± SEM, ##p<0.0001 and **p<0.0001; Kruskal-Wallis test with Dunn's multiple comparisons test).*

4.13. Stimulation of GPR35 receptors using Zaprinast seemed to improve the survival of H9c2 cells exposed to SI/R

To test whether selective agonism of GPR35 receptors protects cardiac cells against SI/R-induced injuries in our experimental setup, cells were treated using Zaprinast to achieve GPR35 receptor activation independently of KYNA administration (*Figure 20A*). Viability measurements revealed that Zaprinast administration improved the survival of cells exposed to SI/R (*Figure 20B*). To further confirm the protective nature of GPR35 receptor agonism, as well as to investigate whether Zaprinast carries KYNA-like antiapoptotic properties in our setting, caspase-3 activation was assessed via western blotting. Here we have shown that exposure to SI/R induced a significant increase in cleaved caspase-3 levels relative to procaspase-3 expression, suggestive of substantial shift towards proapoptotic mechanisms (*Figure 20C-D*). However, although Zaprinast administration decreased the degree of caspase-3 activation compared to that seen in the SI/R+Vehcile group without reaching the level of statistical significance, it is important to emphasize that the SI/R-induced considerable increase in caspase activation diminished when cells received Zaprinast treatment (*Figure 20C-D*).

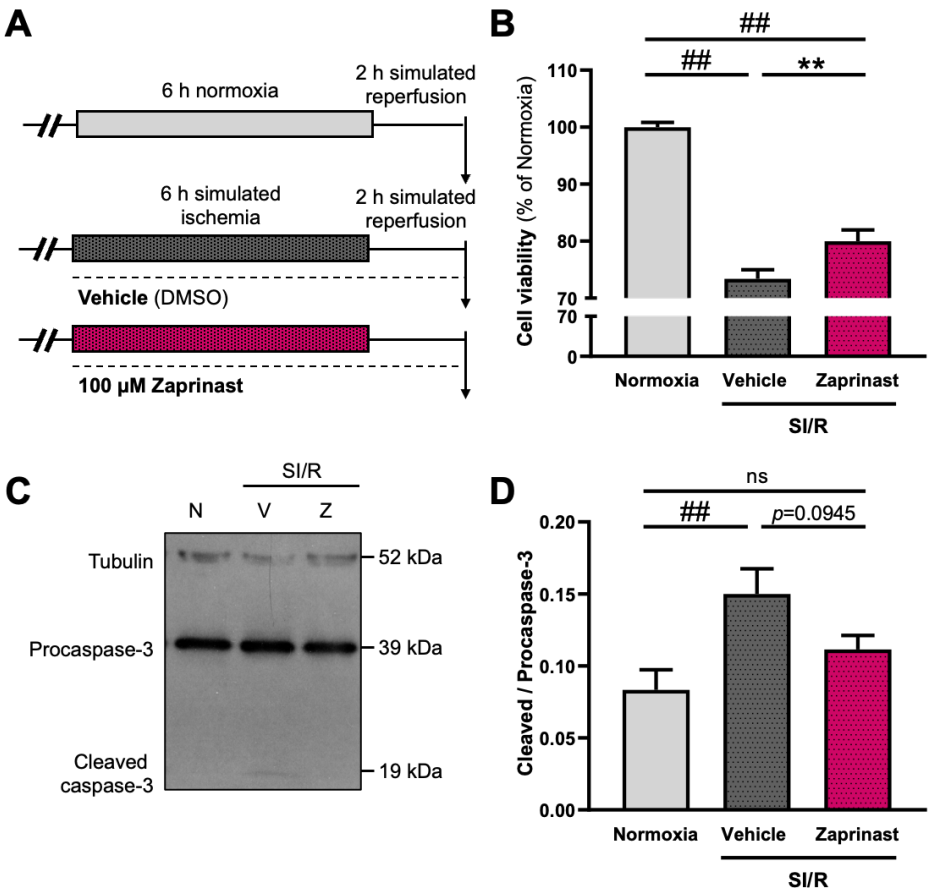

Figure 20. **Zaprinast protected cardiomyoblasts against SI/R-induced cellular injuries.**

*(**A**) Experimental protocol. (**B**) Cell viability in n=14-28/experiment, 5 independent experiments (average cell viability expressed as percentage of average viability in the normoxic group ± SEM, #p<0.01 and **p=0.01; Kruskal-Wallis with Dunn's test). (**C-D**) Representative blot and depiction of caspase-3 activity in n= samples/experiment, 3 independent experiments (average cleaved/procaspase-3 ratio ± SEM, ##p=0.0038; ANOVA with Tukey's multiple comparisons test).*

4.14. GPR35 receptor agonism seemed to maintain mitochondrial respiration

Respiratory functions were assessed then to evaluate whether selective activation of GPR35 receptors improves the functionality of mitochondria in cells exposed to SI/R. Here we have found that the SI/R-induced decrease in baseline O_2 levels diminished upon Zaprinast treatment (*Figure 21A*). In case of OXPHOS-I (*Figure 21B*) and complex-IV (*Figure 21D*) activities, we observed that O_2 flow decreases significantly upon exposure to SI/R, while SI/R was found to tendentiously reduce OXPHOS-II (*Figure 21C*). Importantly, Zaprinast administration improved baseline respiratory parameters, maintaining O_2 consumption rates close to that found in the normoxic controls (*Figure 21A*). Furthermore, KYNA seemed to prevent the SI/R-induced decrease in complex-I-dependent oxidative phosphorylation (*Figure 21B*), as well as to improve complex-IV-linked respiratory capacities substantially (*Figure 21D*).

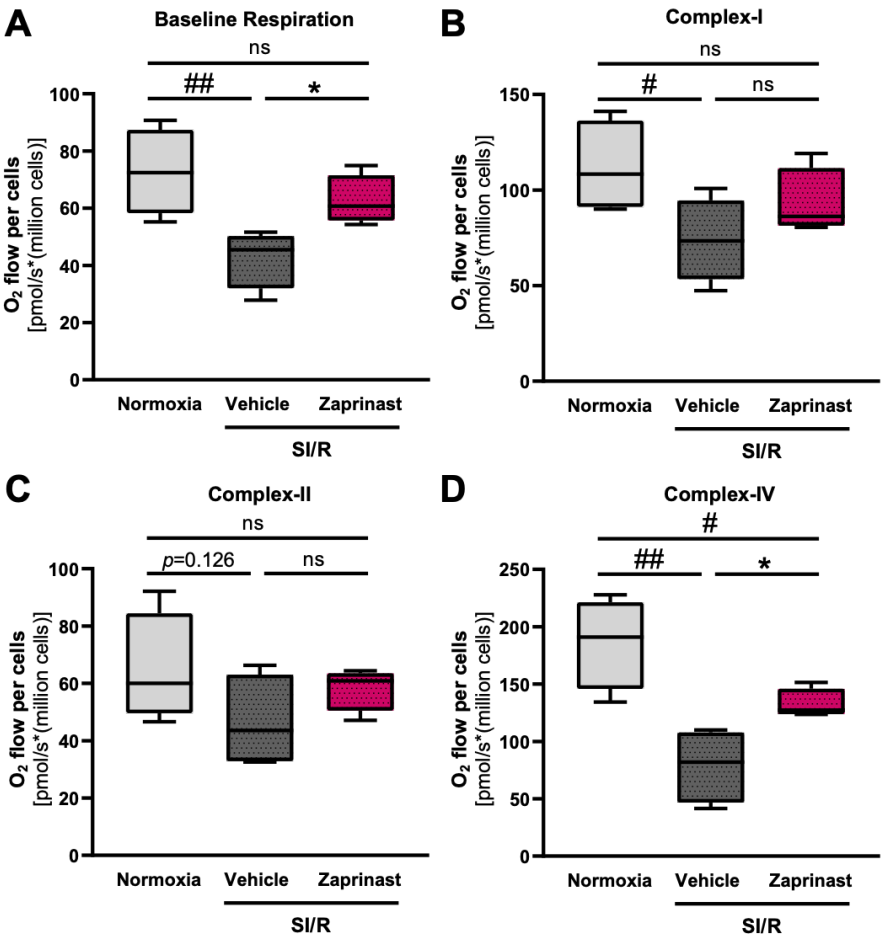

Figure 21. **Zaprinast administration seemed to attenuate the SI/R-induced alterations in parameters of mitochondrial respiration.**

*(**A**) Baseline respiration, (**B**) Complex-I dependent OXPHOS, (**C**) Complex-II dependent OXPHOS and (**D**) Complex-IV dependent OXPHOS in n=4 from 4 separate experiments (average O_2 flow per cell ± SEM, #p<0.05, ##p<0.01 and *p<0.05; ANOVA with Fisher's LSD post hoc test).*

5. Discussion

Despite of basic and clinical research efforts, to date there is no effective therapy ameliorating I/R-induced myocardial tissue damage underlying the deterioration of cardiac functions. KYNA, an endogenously produced Trp metabolite, has been previously shown to exert cardioprotective effects in various models of AMI [67–70]. The thorough mechanism of the KYNA-induced cytoprotection, however, has not been elucidated yet. In the present thesis, we demonstrated that the molecular events laying behind the KYNA-derived protection include antiapoptotic and mitoprotective features. We have also demonstrated that such effects seem to occur at least in part due to GPR35 receptor agonism.

5.1. Novel findings

- Molecular and morphological analyses both revealed that the cytoprotective feature of KYNA in the setting of SI/R occurred in part due to antiapoptotic mechanisms.
- Based on molecular analyses, the suppression of both intrinsic and extrinsic apoptotic pathways seemed to be involved.
- The antiapoptotic property of KYNA seemed to be achieved due to direct inhibition of apoptosis, successfully decreasing camptothecin-induced H9c2 cell damage as well.
- Treatment of H9c2 cells undergoing SI/R with KYNA was found to prevent intramitochondrial calcium accumulation, maintain healthy mitochondrial ultrastructure as well as to preserve the physiological architecture of the mitochondrial network.
- KYNA administration seemed to preserve the functionality of mitochondria in cell cultures exposed to SI/R through decreasing ROS release, preserving the mitochondrial membrane potential and maintaining respiratory capacities.
- The protective nature of KYNA treatment seemed to diminish in presence of parallel GPR35 receptor inhibition, suggesting key GPR35-receptor mediated events along the KYNA-induced cytoprotection.
- Selective GPR35 receptor activation achieved via Zaprinast administration exerted KYNA-like protective effects against SI/R induced cardiac cell death and preserved mitochondrial functions similarly.

5.2. The antiapoptotic feature of KYNA in the setting of SI/R

The propagation of myocardial I/R injury relies on various molecular events, comprising both cell death and survival mechanisms [88, 89]. Besides necrosis, apoptosis is a key contributor to I/R-triggered cardiac cell demise and may serve as a potential target for cardioprotection [12, 24, 89]. The process of programmed cell death is accompanied by

characteristic morphological alterations and a highly ordered sequence of molecular events. Morphological hallmarks include cell shrinkage, membrane blebbing, and impaired nuclear morphology (*e.g.,* DNA condensation and fragmentation, micronuclei formation, appearance of apoptotic bodies) [90, 91]. In the present thesis, we provided several lines of evidence suggesting that H9c2 cardiomyoblasts exhibit these characteristic apoptosis-related morphological alterations upon exposure to SI/R. Our morphological analysis revealed that administration of KYNA seems to suppress the propagation of apoptotic membrane blebbing in cardiac cells exposed to SI/R. Moreover, we have shown that KYNA treatment reduced the number of cell nuclei exhibiting apoptotic-like morphology. Similarly to our findings, KYNA has been demonstrated to preserve nuclear morphology in a model of Parkinson's disease as well [92]. These results suggest that apoptotic-like morphological changes can be delayed, reduced, or even reverted upon treatment with KYNA.

With regards to molecular events along the course of apoptosis, we have found that KYNA reduced the SI/R-induced shift towards proapoptotic mechanisms. When investigating the intrinsic apoptotic pathway, we have observed that KYNA administration seems to revert the SI/R-induced significant increase in the expression of BAX, a core proapoptotic regulatory protein. Furthermore, levels of antiapoptotic Bcl-XL were found to increase substantially upon KYNA treatment in cells subjected to SI/R. Bcl-2 levels were shown to increase tendentiously upon KYNA administration without reaching the level of statistical significance. In summary, our results suggest that KYNA alters the expression of mediators regulating the activation of intrinsic apoptosis. These findings are in line with observations reported by Lee *et al.*, proposing that the neuroprotective feature of KYNA in an *in vitro* model of Parkinson's disease involves the downregulation of BAX expression [92]. With regards to extrinsic apoptotic mechanisms, we investigated caspase-8 activity, responsible for the conduction of extrinsic apoptosis initiation. Our analysis revealed that KYNA decreased the baseline expression of its zymogen form (*i.e.,* procaspase-8) significantly, in parallel with reduction of its SI/R-induced activation (*i.e.,* cleaved caspase-8). These results support the idea that KYNA impacts extrinsic apoptosis initiation as well. Apart from apoptosis initiation, our investigations on the common executionary pathway revealed that caspase-3 and -7 activities increased substantially in cells subjected to SI/R, which effect was found to diminish upon KYNA treatment, confirming that KYNA seems to evoke antiapoptotic features in the setting of myocardial I/R. Further supporting these observations, we also demonstrated that in cardiac cells treated with the apoptosis-inducer camptothecin KYNA exerted antiapoptotic effects. These observations are in line with previous reports demonstrating that KYNA exhibits antiapoptotic potential in the

central nervous system through inhibiting the activation of executionary caspases. Meller *et al.* reported that KYNA withdrawal elicits increased caspase activation and consequent neuronal apoptosis in an *in vitro* model of epilepsy [93]. In addition, pre-treatment of SH-SY5Y and SK-N-SH cells with KYNA was shown to reduce the 1-methyl-4-phenylpyridinium-induced neuronal cell death through the attenuation of caspase-9/-3 activities in an *in vitro* model of Parkinson's disease [92].

Based on these results, we propose that the cytoprotective effect of KYNA in the setting of myocardial I/R involves antiapoptotic mechanisms, inhibiting the propagation of both intrinsic and extrinsic apoptotic pathways, along with the execution of programmed cell death.

5.3. The role of mitoprotection in the KYNA-triggered cardiocytoprotection

Mitochondrial dysfunction is a fundamental event along the development of cardiac I/R-injuries, accompanied by various molecular mechanisms, including Ca^{2+} buildup, membrane depolarization and release of mitochondrial matrix constituents into the cytosol [28, 33]. Importantly, mitochondrial impairment may trigger various cell death mechanisms, depending on the severity of the condition, being a fundamental factor along apoptosis initiation [22, 23].

Intramitochondrial Ca^{2+} overload triggers a sequence of events damaging mitochondria further. These include increased release of ROS, as well as mtPTP opening and consequent mitochondrial membrane depolarization, ultimately leading to cytochrome-C release and initiation of the intrinsic apoptotic pathway [94, 95]. Our results demonstrated that H9c2 cells showed significantly increased intramitochondrial Ca^{2+} levels upon subjection to SI/R. KYNA treatment, however, was shown to reduce the mitochondrial Ca^{2+} content in cells undergoing SI/R. Considering that mitochondrial Ca^{2+} buildup is a key trigger of intrinsic apoptosis, these results are in line with our previous observations demonstrating antiapoptotic effects. Further confirming our results, previous reports have demonstrated that KYNA administration suppresses the NMDA-induced increase of intracellular Ca^{2+} levels in cultured astrocytes expressing GluN1 subunit-containing NMDA receptors [96].

Keeping in mind that intramitochondrial Ca^{2+} accumulation promotes prolonged mtPTP opening, causing mitochondrial swelling, ultimately leading to rupture of mitochondrial membranes [97, 98], we assessed whether KYNA treatment impacts the SI/R-induced ultrastructural changes. Our results obtained through morphometric analysis on electron microscopic images revealed that mitochondria in cells exposed to SI/R show significantly increased aspect ratio, Feret's diameter, perimeter and average area, in parallel with decreased circularity, suggestive of swelling and elongation of mitochondria [80, 99]. KYNA treatment,

on the other hand, was shown to preserve healthy mitochondrial morphology in cells undergoing SI/R. The architecture of the mitochondrial network was visualized then using MitoTracking to further corroborate that KYNA improves the SI/R-induced deteriorations in the arrangement of mitochondria. Here, KYNA treatment was found to reduce the ratio of cells exhibiting aggregate-like structures in their mitochondrial network.

Next, we investigated potential molecular mechanisms laying behind the observed morphological alterations. Here, we focused on the involvement of mitochondrial quality control mechanisms. These consist of multiple coordinated pathways such as fusion and fission of mitochondria, determining the arrangement of the mitochondrial network, maintaining cellular mitochondrial homeostasis [100–102]. Our results demonstrated that SI/R-induced a substantial increase in the transcription of genes encoding both profusion and fission-driving mediators. This effect seemed to diminish upon KYNA treatment. Interestingly, these changes were not yet detectable on the level of protein expression. Although we have not examined this phenomenon further yet, it seems plausible that altered mitochondrial quality control mechanisms have not contributed to the observed morphological alterations. Nevertheless, increased mRNA levels may support the idea that both fusion and fission contribute to late-onset injuries of cardiac cells following I/R, which could be prevented by KYNA administration. Other mechanisms laying behind unaffected protein levels (*e.g.,* potential post-transcriptional regulatory mechanisms suppressing the effects of SI/R and KYNA on the expression of fusion- and fission-driving proteins) remain to be investigated.

Recent discoveries demonstrated that the changes in mitochondrial morphology, as well as altered arrangement of mitochondria correlate with both cellular energy status and mitochondrial functions [103–105]. These impairments have been associated with enhanced mitochondrial ROS production, contributing to the AMI-induced damage of cardiac cells [101, 106]. Previously, it has been demonstrated that KYNA exhibits antioxidant effects in neuronal and hepatic tissues [56, 65]. In line with these observations, we have previously shown that KYNA treatment attenuates the SI/R-triggered increase in cellular superoxide levels [70]. To further clarify the KYNA-derived antioxidant effects in the setting of SI/R, we examined whether KYNA impacts mitochondrial ROS production in cardiac cells undergoing SI/R. Here we have found that KYNA administration significantly decreased the degree of SI/R-triggered mitochondrial superoxide release. These results are in line with recent observations on neonatal mouse cardiomyocyte cultures subjected to SI/R [69]. Further supporting the antioxidant role of KYNA, it has been reported that its administration prevents the I/R-induced decrease in the expression of superoxide dismutase 2 enzyme [67].

As increased oxidative stress contributes to the collapse of the mitochondrial membrane potential, a key event of I/R-induced cardiac cell damage [107, 108], next we examined the potential effects of KYNA on the SI/R-induced mitochondrial membrane depolarization. Our results provided evidence suggesting that KYNA administration prevents the SI/R-induced loss of mitochondrial membrane potential. This observation is in accordance with findings reporting similar KYNA-derived effects using a different approach in another H9c2 cell-based model of myocardial I/R [67]. To further support that KYNA maintains the functionality of mitochondria, respiratory capacities were examined. KYNA administered throughout SI/R has been found to improve baseline oxygen consumption of cells subjected to SI/R. Furthermore, it was shown to reduce the degree of SI/R-induced impairments of complex-I, -II and -IV-linked respirations, improving O_2 consumption rates in all examined respiratory states. Similar KYNA-derived effects have been reported by Poles *et al*., demonstrating improved respiratory functions in a rat model of sepsis-associated mitochondrial impairment in the nervous tissue [109]. Interestingly, contradictory findings have been published as well with regards to the effects of KYNA on mitochondrial functions. Administration of KYNA (≥ 125 μmol/L) to mitochondria isolated from cardiac cells has been found to impair mitochondrial function as well as to lower ATP production [45]. Moreover, it has been demonstrated that neither subjection of cardiac cells to I/R nor KYNA administration alters the expression of respiratory chain complex constituent proteins and their activities [67]. Nevertheless, our results support the idea that KYNA improves mitochondrial functions in the setting of SI/R, in accordance with findings of Wyant *et al.*, reporting that providing KYNA treatment prevents the ischemia-induced ATP depletion in IPS-derived cardiomyocytes exposed to I/R [69].

5.4. The significance of GPR35 receptor agonism in the KYNA-induced protection of cardiac cells against I/R-injuries

Receptor-mediated modulation of intracellular signaling pathways is the most likely mechanism laying behind the KYNA-derived effects. The metabolite is known to exert an antagonistic effect on ionotropic glutamate receptors, such as NMDA and AMPA receptors, as well as to activate AhR and GPR35 receptors. Although the widely investigated KYNA-derived neuroprotective features have been mostly attributed to the metabolite's NMDA receptor antagonistic properties [12,49], our previous studies demonstrated that blocking NMDA receptor activity selectively has not been found to impact the survival of cardiac cells undergoing SI/R significantly [70]. Among another KYNA target receptors, GPR35 receptors have been reported to exert promising effects considering potential cardioprotective

mechanisms. It has been recently demonstrated that the KYNA-induced GPR35 receptor agonism seems to prevent the ischemia-induced ATP loss [69]. GPR35 receptor agonism related protective effects against I/R-injuries have been identified outside of the cardiovascular system as well (*e.g.*, in the central nervous system), further supporting the idea GPR35 receptor activation may be a key event along the KYNA-induced protective mechanisms [110]. On the other hand, others reported controversial data with regards to the role of GPR35 receptors. For example, Chen *et al.* reported that downregulation of GPR35 receptor activation reduces the degree of ischemia-induced oxidative stress, and preserves mitochondrial functions, thereby preventing the propagation of mitochondria-dependent intrinsic apoptosis and protecting the cardiac tissue against ischemic injury [111]. In addition, stimulation of GPR35 receptors have been demonstrated to increase ROS generation, aggravating oxidative stress [112]. To address these contradictory observations, we proposed investigations to uncover whether GPR35 receptor agonism has an important role in the cardiocytoprotective effect of KYNA. First, we assessed whether KYNA exerts cardioprotection when applied in parallel with CID2745687, a well-known GPR35 receptor antagonist. Here, although KYNA has been shown to achieve significant cytoprotection when administered alone, we have found that inhibition of GPR35 receptor activity via simultaneous treatment with CID2745687 diminished the KYNA-induced cytoprotection. Next, we examined whether selective GPR35 receptor stimulation using Zaprinast, a synthetic agonist achieves protective effects. Our results demonstrated that Zaprinast treatment significantly improved the survival of H9c2 cardiac cells undergoing SI/R. Furthermore, Zaprinast administration was found to prevent the SI/R-induced substantial increase in caspase-3 activation, suggesting potential GPR35 receptor triggered antiapoptotic mechanisms. Additionally, we have shown that Zaprinast treatment seems to preserve the functionality of mitochondria, similarly to that found in case of KYNA administration. These observations suggest that the KYNA-derived cyto- and mitoprotection seems to occur at least in part due to the GPR35 receptor agonistic feature of KYNA. Taken together, our results suggest that GPR35 receptor agonism seems to play a fundamental role in the KYNA-mediated protection of cardiac cells against the SI/R-induced deterioration. Nevertheless, considering that Zaprinast treatment was found to trigger less pronounced protective effects in our experimental setup (*e.g.*, less pronounced effects on respiratory capacities), it is likely that the KYNA-driven protection against I/R-injury involves further molecular mechanisms besides those aggravated by stimulation of GPR35 receptors.

5.5. Limitations

Although we have provided several lines of evidence to reveal the mechanism laying behind the KYNA-driven protection against I/R-induced myocardial injuries, our work is not without limitations. Firstly, our results rely on *in vitro* based experiments using cardiomyoblasts. Hence, our observations are limited to demonstrate potential further aspects of the KYNA-derived beneficial effects that may arise through the protection of either differentiated, adult-type cardiomyocytes or other cell types found in the myocardium (*e.g.,* endothelial cells, fibroblasts). Nonetheless, some of our results have been recently corroborated by others using *ex vivo* and *in vivo* settings. Secondly, our investigations focused on the analysis of antiapoptotic and mitoprotective effects. Further types of cell death (e.g., necroptosis, pyroptosis, autophagy-triggered cell death) must be assessed, however, to understand the precise mechanisms of action laying behind the observed effects of KYNA. Thirdly, additional investigations are required to clarify whether other KYNA target receptors (*i.e.,* AhR, AMPA, or kainate receptors) are involved in the KYNA-mediated protection of cardiac cells. Lastly, we have provided evidence that KYNA triggers protection when administrated throughout the period of I/R. Other setups, involving either pre- or post-I/R treatment regimens should be tested in the future to identify the most sufficient type of application. Also, it should be examined further if KYNA exerts any significant effects on mitochondrial structure and function under normoxia. Nevertheless, we have provided novel details on the mechanism of action of the KYNA-derived cardiocytoprotection in the setting of myocardial I/R.

6. Summary

Cardiovascular diseases, including AMI, are leading causes of death globally. KYNA has been previously shown to improve the survival of cardiac cells exposed to I/R, however, the mechanisms laying behind protective feature of KYNA in the setting of myocardial I/R have not been clarified yet. Hence, our aim was to uncover molecular events enabling the KYNA-derived cardioprotection.

In the present thesis, we have demonstrated that KYNA shows antiapoptotic and mitoprotective effects in the setting of SI/R. Based on our findings, the KYNA-induced protection seems to involve the suppression of both intrinsic and extrinsic apoptotic pathways, as well as the maintenance of physiological intramitochondrial Ca^{2+} levels, preservation of the structural and functional integrity of mitochondria, and reduction of mitochondrial oxidative stress. Furthermore, we have provided evidence suggesting that survival and mitochondrial respiration of cardiac cells treated with Zaprinast (*i.e.,* another GPR35 receptor agonist) improved significantly, while inhibition of GPR35 receptor activity in parallel with KYNA treatment diminished the KYNA-induced cytoprotection, suggesting that stimulation of GPR35 receptor mediated pathways make substantial contributions to the protective effects of KYNA. As mitochondrial impairment is a cornerstone of cardiac injury and a driver of I/R-induced proapoptotic mechanisms, our results demonstrating the mitoprotective features of KYNA in the setting of cardiac I/R injury might contribute to the improvement of novel treatment strategies for AMI patients.

However, future development of cardioprotective drugs based on the beneficial mechanisms triggered by KYNA requires further investigations, including analysis of additional molecular pathways involved, or efficiency in other animal models. As for safe applicability, previously we have shown that KYNA administration under stress-free conditions does not impact cell viability [70], suggesting safe applicability. This idea is supported by the fact that various cells have been reported to tolerate even higher KYNA concentrations [113, 114]. Although systemic KYNA administration has not been tested on humans, a phase-1 randomized double-blind clinical trial supported safety and tolerability of topically delivered KYNA [115]. Nevertheless, pharmacokinetics following systemic administration, as well as optimal routes of delivery (*e.g.,* application of exogenous KYNA or stimulation of endogenous KYNA synthesis via altering the activities of enzymes governing the KP) remain to be examined. Nevertheless, as a natural, endogenously synthesized compound, KYNA seems to be a promising candidate for the future development of cardioprotective drugs.

7. Bibliography

1. Knuuti J, Wijns W, Saraste A, et al (2020) 2019 ESC Guidelines for the diagnosis and management of chronic coronary syndromes. Eur Heart J 41:407–477. https://doi.org/10.1093/eurheartj/ehz425

2. Byrne RA, Rossello X, Coughlan JJ, et al (2023) 2023 ESC Guidelines for the management of acute coronary syndromes. Eur Heart J 44:3720–3826. https://doi.org/10.1093/eurheartj/ehad191

3. Buja LM (2005) Myocardial ischemia and reperfusion injury. Cardiovasc Pathol 14:170–175. https://doi.org/10.1016/j.carpath.2005.03.006

4. Reddy K, Khaliq A, Henning RJ (2015) Recent advances in the diagnosis and treatment of acute myocardial infarction. World J Cardiol 7:243–276. https://doi.org/10.4330/wjc.v7.i5.243

5. Welt FGP, Batchelor W, Spears JR, et al (2024) Reperfusion Injury in Patients With Acute Myocardial Infarction: JACC Scientific Statement. Journal of the American College of Cardiology 83:2196–2213. https://doi.org/10.1016/j.jacc.2024.02.056

6. Kalogeris T, Baines CP, Krenz M, Korthuis RJ (2016) Ischemia/Reperfusion. Compr Physiol 7:113–170. https://doi.org/10.1002/cphy.c160006

7. de Groot H, Rauen U (2007) Ischemia-reperfusion injury: processes in pathogenetic networks: a review. Transplant Proc 39:481–484. https://doi.org/10.1016/j.transproceed.2006.12.012

8. Sanada S, Komuro I, Kitakaze M (2011) Pathophysiology of myocardial reperfusion injury: preconditioning, postconditioning, and translational aspects of protective measures. Am J Physiol Heart Circ Physiol 301:H1723-1741. https://doi.org/10.1152/ajpheart.00553.2011

9. Morciano G, Bonora M, Campo G, et al (2017) Mechanistic Role of mPTP in Ischemia-Reperfusion Injury. Adv Exp Med Biol 982:169–189. https://doi.org/10.1007/978-3-319-55330-6_9

10. Bernardi P, Gerle C, Halestrap AP, et al (2023) Identity, structure, and function of the mitochondrial permeability transition pore: controversies, consensus, recent advances, and future directions. Cell Death Differ 30:1869–1885. https://doi.org/10.1038/s41418-023-01187-0

11. Du B, Fu Q, Yang Q, et al (2025) Different types of cell death and their interactions in myocardial ischemia–reperfusion injury. Cell Death Discov 11:87. https://doi.org/10.1038/s41420-025-02372-5

12. McCully JD, Wakiyama H, Hsieh Y-J, et al (2004) Differential contribution of necrosis and apoptosis in myocardial ischemia-reperfusion injury. Am J Physiol Heart Circ Physiol 286:H1923-1935. https://doi.org/10.1152/ajpheart.00935.2003

13. Piper HM, Meuter K, Schäfer C (2003) Cellular mechanisms of ischemia-reperfusion injury. The Annals of Thoracic Surgery 75:S644–S648. https://doi.org/10.1016/S0003-4975(02)04686-6

14. Gottlieb RA (2011) Cell Death Pathways in Acute Ischemia/Reperfusion Injury. J Cardiovasc Pharmacol Ther 16:233–238. https://doi.org/10.1177/1074248411409581

15. Xiang Q, Yi X, Zhu X-H, et al (2024) Regulated cell death in myocardial ischemia–reperfusion injury. Trends in Endocrinology & Metabolism 35:219–234. https://doi.org/10.1016/j.tem.2023.10.010

16. Du B, Fu Q, Yang Q, et al (2025) Different types of cell death and their interactions in myocardial ischemia–reperfusion injury. Cell Death Discov 11:87. https://doi.org/10.1038/s41420-025-02372-5

17. Pinci F, Gaidt MM, Jung C, et al (2022) Tumor necrosis factor is a necroptosis-associated alarmin. Front Immunol 13:. https://doi.org/10.3389/fimmu.2022.1074440

18. Frank D, Vince JE (2019) Pyroptosis versus necroptosis: similarities, differences, and crosstalk. Cell Death Differ 26:99–114. https://doi.org/10.1038/s41418-018-0212-6

19. Rao Z, Zhu Y, Yang P, et al (2022) Pyroptosis in inflammatory diseases and cancer. Theranostics 12:4310–4329. https://doi.org/10.7150/thno.71086

20. Savitskaya MA, Onishchenko GE (2015) Mechanisms of Apoptosis. Biochemistry (Mosc) 80:1393–1405. https://doi.org/10.1134/S0006297915110012

21. Elmore S (2007) Apoptosis: a review of programmed cell death. Toxicol Pathol 35:495–516. https://doi.org/10.1080/01926230701320337

22. D'Arcy MS (2019) Cell death: a review of the major forms of apoptosis, necrosis and autophagy. Cell Biology International 43:582–592. https://doi.org/10.1002/cbin.11137

23. Gottlieb RA, Engler RL (1999) Apoptosis in myocardial ischemia-reperfusion. Ann N Y Acad Sci 874:412–426. https://doi.org/10.1111/j.1749-6632.1999.tb09255.x

24. Eefting F, Rensing B, Wigman J, et al (2004) Role of apoptosis in reperfusion injury. Cardiovasc Res 61:414–426. https://doi.org/10.1016/j.cardiores.2003.12.023

25. Lee Y, Gustafsson ÅB (2009) Role of apoptosis in cardiovascular disease. Apoptosis 14:536–548. https://doi.org/10.1007/s10495-008-0302-x

26. Kim G-T, Chun Y-S, Park J-W, Kim M-S (2003) Role of apoptosis-inducing factor in myocardial cell death by ischemia–reperfusion. Biochemical and Biophysical Research Communications 309:619–624. https://doi.org/10.1016/j.bbrc.2003.08.045

27. Wang J, Toan S, Zhou H (2020) New insights into the role of mitochondria in cardiac microvascular ischemia/reperfusion injury. Angiogenesis 23:299–314. https://doi.org/10.1007/s10456-020-09720-2

28. Honda HM, Korge P, Weiss JN (2005) Mitochondria and Ischemia/Reperfusion Injury. Annals of the New York Academy of Sciences 1047:248–258. https://doi.org/10.1196/annals.1341.022

29. Perrelli M-G, Pagliaro P, Penna C (2011) Ischemia/reperfusion injury and cardioprotective mechanisms: Role of mitochondria and reactive oxygen species. World J Cardiol 3:186–200. https://doi.org/10.4330/wjc.v3.i6.186

30. Marin W, Marin D, Ao X, Liu Y (2021) Mitochondria as a therapeutic target for cardiac ischemia-reperfusion injury (Review). Int J Mol Med 47:485–499. https://doi.org/10.3892/ijmm.2020.4823

31. Marin W, Marin D, Ao X, Liu Y (2021) Mitochondria as a therapeutic target for cardiac ischemia-reperfusion injury (Review). International Journal of Molecular Medicine 47:485–499. https://doi.org/10.3892/ijmm.2020.4823

32. Wu M, Gu X, Ma Z (2021) Mitochondrial Quality Control in Cerebral Ischemia–Reperfusion Injury. Mol Neurobiol 58:5253–5271. https://doi.org/10.1007/s12035-021-02494-8

33. Kuznetsov AV, Javadov S, Margreiter R, et al (2019) The Role of Mitochondria in the Mechanisms of Cardiac Ischemia-Reperfusion Injury. Antioxidants (Basel) 8:454. https://doi.org/10.3390/antiox8100454

34. Serasinghe MN, Chipuk JE (2017) Mitochondrial Fission in Human Diseases. Handb Exp Pharmacol 240:159–188. https://doi.org/10.1007/164_2016_38

35. Nan J, Zhu W, Rahman MS, et al (2017) Molecular regulation of mitochondrial dynamics in cardiac disease. Biochimica et Biophysica Acta (BBA) - Molecular Cell Research 1864:1260–1273. https://doi.org/10.1016/j.bbamcr.2017.03.006

36. Hausenloy DJ, Yellon DM (2011) The therapeutic potential of ischemic conditioning: an update. Nat Rev Cardiol 8:619–629. https://doi.org/10.1038/nrcardio.2011.85

37. Richard DM, Dawes MA, Mathias CW, et al (2009) L-Tryptophan: Basic Metabolic Functions, Behavioral Research and Therapeutic Indications. Int J Tryptophan Res 2:45–60. https://doi.org/10.4137/ijtr.s2129

38. Gao A, Qi Y, Luo Y, et al (2025) Mass spectrometric monitoring of redox transformation and arylation of tryptophan. Analytica Chimica Acta 1349:343822. https://doi.org/10.1016/j.aca.2025.343822

39. Xue C, Li G, Zheng Q, et al (2023) Tryptophan metabolism in health and disease. Cell Metabolism 35:1304–1326. https://doi.org/10.1016/j.cmet.2023.06.004

40. Badawy AA-B (2017) Kynurenine Pathway of Tryptophan Metabolism: Regulatory and Functional Aspects. Int J Tryptophan Res 10:1178646917691938. https://doi.org/10.1177/1178646917691938

41. Gáspár R, Halmi D, Demján V, et al (2021) Kynurenine Pathway Metabolites as Potential Clinical Biomarkers in Coronary Artery Disease. Front Immunol 12:768560. https://doi.org/10.3389/fimmu.2021.768560

42. Wang Z, Xie X, Xue Y, Chen Y (2025) Tryptophan-2,3-Dioxygenase as a Therapeutic Target in Digestive System Diseases. Biology 14:295. https://doi.org/10.3390/biology14030295

43. Al-Abdallah B, Al-Faiyz YS, Shaaban S (2022) Anticancer, Antimicrobial, and Antioxidant Activities of Organodiselenide-Tethered Methyl Anthranilates. Biomolecules 12:1765. https://doi.org/10.3390/biom12121765

44. Milusheva M, Todorova M, Gledacheva V, et al (2023) Novel Anthranilic Acid Hybrids—An Alternative Weapon against Inflammatory Diseases. Pharmaceuticals (Basel) 16:1660. https://doi.org/10.3390/ph16121660

45. Baran H, Amann G, Lubec B, Lubec G (1997) Kynurenic acid and kynurenine aminotransferase in heart. Pediatr Res 41:404–410. https://doi.org/10.1203/00006450-199703000-00017

46. Tóth F, Cseh EK, Vécsei L (2021) Natural Molecules and Neuroprotection: Kynurenic Acid, Pantethine and α-Lipoic Acid. Int J Mol Sci 22:403. https://doi.org/10.3390/ijms22010403

47. Vamos E, Pardutz A, Klivenyi P, et al (2009) The role of kynurenines in disorders of the central nervous system: possibilities for neuroprotection. J Neurol Sci 283:21–27. https://doi.org/10.1016/j.jns.2009.02.326

48. Wirthgen E, Hoeflich A, Rebl A, Günther J (2018) Kynurenic Acid: The Janus-Faced Role of an Immunomodulatory Tryptophan Metabolite and Its Link to Pathological Conditions. Front Immunol 8:. https://doi.org/10.3389/fimmu.2017.01957

49. Alves L de F, Moore JB, Kell DB (2024) The Biology and Biochemistry of Kynurenic Acid, a Potential Nutraceutical with Multiple Biological Effects. Int J Mol Sci 25:9082. https://doi.org/10.3390/ijms25169082

50. Moroni F, Cozzi A, Sili M, Mannaioni G (2012) Kynurenic acid: a metabolite with multiple actions and multiple targets in brain and periphery. J Neural Transm (Vienna) 119:133–139. https://doi.org/10.1007/s00702-011-0763-x

51. Walczak K, Wnorowski A, Turski WA, Plech T (2020) Kynurenic acid and cancer: facts and controversies. Cell Mol Life Sci 77:1531–1550. https://doi.org/10.1007/s00018-019-03332-w

52. Wirthgen E, Hoeflich A, Rebl A, Günther J (2017) Kynurenic Acid: The Janus-Faced Role of an Immunomodulatory Tryptophan Metabolite and Its Link to Pathological Conditions. Front Immunol 8:1957. https://doi.org/10.3389/fimmu.2017.01957

53. Cosi C, Mannaioni G, Cozzi A, et al (2011) G-protein coupled receptor 35 (GPR35) activation and inflammatory pain: Studies on the antinociceptive effects of kynurenic acid and zaprinast. Neuropharmacology 60:1227–1231. https://doi.org/10.1016/j.neuropharm.2010.11.014

54. Agudelo LZ, Ferreira DMS, Cervenka I, et al (2018) Kynurenic Acid and Gpr35 Regulate Adipose Tissue Energy Homeostasis and Inflammation. Cell Metab 27:378-392.e5. https://doi.org/10.1016/j.cmet.2018.01.004

55. Zhen D, Liu J, Zhang XD, Song Z (2022) Kynurenic Acid Acts as a Signaling Molecule Regulating Energy Expenditure and Is Closely Associated With Metabolic Diseases. Front Endocrinol (Lausanne) 13:847611. https://doi.org/10.3389/fendo.2022.847611

56. Sun T, Xie R, He H, et al (2022) Kynurenic acid ameliorates NLRP3 inflammasome activation by blocking calcium mobilization via GPR35. Front Immunol 13:1019365. https://doi.org/10.3389/fimmu.2022.1019365

57. Lugo-Huitrón R, Blanco-Ayala T, Ugalde-Muñiz P, et al (2011) On the antioxidant properties of kynurenic acid: free radical scavenging activity and inhibition of oxidative stress. Neurotoxicol Teratol 33:538–547. https://doi.org/10.1016/j.ntt.2011.07.002

58. Bratek-Gerej E, Ziembowicz A, Godlewski J, Salinska E (2021) The Mechanism of the Neuroprotective Effect of Kynurenic Acid in the Experimental Model of Neonatal Hypoxia–Ischemia: The Link to Oxidative Stress. Antioxidants 10:1775. https://doi.org/10.3390/antiox10111775

59. Andiné P, Lehmann A, Ellrén K, et al (1988) The excitatory amino acid antagonist kynurenic acid administered after hypoxic-ischemia in neonatal rats offers neuroprotection. Neurosci Lett 90:208–212. https://doi.org/10.1016/0304-3940(88)90813-0

60. Li G, Li S, Zhou W (2025) Kynurenine pathway: a possible new mechanism for exercise in the prevention and treatment of Alzheimer's disease. Front Aging Neurosci 17:. https://doi.org/10.3389/fnagi.2025.1617690

61. Nahomi RB, Nam M-H, Rankenberg J, et al (2020) Kynurenic Acid Protects Against Ischemia/Reperfusion-Induced Retinal Ganglion Cell Death in Mice. Int J Mol Sci 21:1795. https://doi.org/10.3390/ijms21051795

62. Ostapiuk A, Urbanska EM (2021) Kynurenic acid in neurodegenerative disorders—unique neuroprotection or double-edged sword? CNS Neurosci Ther 28:19–35. https://doi.org/10.1111/cns.13768

63. Wang D, Li D, Zhang Y, et al (2021) Functional metabolomics reveal the role of AHR/GPR35 mediated kynurenic acid gradient sensing in chemotherapy-induced intestinal damage. Acta Pharm Sin B 11:763–780. https://doi.org/10.1016/j.apsb.2020.07.017

64. Wang Y, Liu Z, Shen P, et al (2022) Kynurenic acid ameliorates lipopolysaccharide-induced endometritis by regulating the GRP35/NF-κB signaling pathway. Toxicol Appl Pharmacol 438:115907. https://doi.org/10.1016/j.taap.2022.115907

65. Marciniak S, Wnorowski A, Smolińska K, et al (2018) Kynurenic Acid Protects against Thioacetamide-Induced Liver Injury in Rats. Anal Cell Pathol (Amst) 2018:1270483. https://doi.org/10.1155/2018/1270483

66. Pyun DH, Kim TJ, Kim MJ, et al (2021) Endogenous metabolite, kynurenic acid, attenuates nonalcoholic fatty liver disease via AMPK/autophagy- and AMPK/ORP150-mediated signaling. J Cell Physiol 236:4902–4912. https://doi.org/10.1002/jcp.30199

67. Kamel R, Baetz D, Gueguen N, et al (2023) Kynurenic Acid: A Novel Player in Cardioprotection against Myocardial Ischemia/Reperfusion Injuries. Pharmaceuticals 16:1381. https://doi.org/10.3390/ph16101381

68. Olenchock BA, Moslehi J, Baik AH, et al (2016) EGLN1 Inhibition and Rerouting of α-Ketoglutarate Suffice for Remote Ischemic Protection. Cell 164:884–895. https://doi.org/10.1016/j.cell.2016.02.006

69. Wyant GA, Yu W, Doulamis IiP, et al (2022) Mitochondrial remodeling and ischemic protection by G protein-coupled receptor 35 agonists. Science 377:621–629. https://doi.org/10.1126/science.abm1638

70. Gáspár R, Nógrádi-Halmi D, Demján V, et al (2024) Kynurenic acid protects against ischemia/reperfusion injury by modulating apoptosis in cardiomyocytes. Apoptosis 29:1483–1498. https://doi.org/10.1007/s10495-024-02004-w

71. Choi J-H, Kim D-H, Yun I-J, et al (2007) Zaprinast inhibits hydrogen peroxide-induced lysosomal destabilization and cell death in astrocytes. Eur J Pharmacol 571:106–115. https://doi.org/10.1016/j.ejphar.2007.06.042

72. Schütte H, Witzenrath M, Mayer K, et al (2000) The PDE inhibitor zaprinast enhances NO-mediated protection against vascular leakage in reperfused lungs. Am J Physiol Lung Cell Mol Physiol 279:L496-502. https://doi.org/10.1152/ajplung.2000.279.3.L496

73. Atkin-Smith GK, Poon IKH (2017) Disassembly of the Dying: Mechanisms and Functions. Trends in Cell Biology 27:151–162. https://doi.org/10.1016/j.tcb.2016.08.011

74. Mills JC, Stone NL, Erhardt J, Pittman RN (1998) Apoptotic membrane blebbing is regulated by myosin light chain phosphorylation. J Cell Biol 140:627–636. https://doi.org/10.1083/jcb.140.3.627

75. Ziegler U, Groscurth P (2004) Morphological features of cell death. News Physiol Sci 19:124–128. https://doi.org/10.1152/nips.01519.2004

76. Tixeira R, Phan TK, Caruso S, et al (2020) ROCK1 but not LIMK1 or PAK2 is a key regulator of apoptotic membrane blebbing and cell disassembly. Cell Death Differ 27:102–116. https://doi.org/10.1038/s41418-019-0342-5

77. Gáspár R, Pipicz M, Hawchar F, et al (2016) The cytoprotective effect of biglycan core protein involves Toll-like receptor 4 signaling in cardiomyocytes. J Mol Cell Cardiol 99:138–150. https://doi.org/10.1016/j.yjmcc.2016.08.006

78. Mayhew TM (1992) A review of recent advances in stereology for quantifying neural structure. J Neurocytol 21:313–328. https://doi.org/10.1007/BF01191700

79. Pajer K, Bellák T, Grósz T, et al (2023) Riluzole treatment modulates KCC2 and EAAT-2 receptor expression and Ca2+ accumulation following ventral root avulsion injury. Eur J Cell Biol 102:151317. https://doi.org/10.1016/j.ejcb.2023.151317

80. Nogradi B, Meszlenyi V, Patai R, et al (2020) Diazoxide blocks or reduces microgliosis when applied prior or subsequent to motor neuron injury in mice. Brain Research 1741:146875. https://doi.org/10.1016/j.brainres.2020.146875

81. Demeter-Haludka V, Kovács M, Petrus A, et al (2018) Examination of the Role of Mitochondrial Morphology and Function in the Cardioprotective Effect of Sodium Nitrite Administered 24 h Before Ischemia/Reperfusion Injury. Front Pharmacol 9:. https://doi.org/10.3389/fphar.2018.00286

82. Errea O, Moreno B, Gonzalez-Franquesa A, et al (2015) The disruption of mitochondrial axonal transport is an early event in neuroinflammation. Journal of Neuroinflammation 12:152. https://doi.org/10.1186/s12974-015-0375-8

83. Johnson D, Nehrke K (2010) Mitochondrial Fragmentation Leads to Intracellular Acidification in Caenorhabditis elegans and Mammalian Cells. Mol Biol Cell 21:2191–2201. https://doi.org/10.1091/mbc.E09-10-0874

84. Djafarzadeh S, Jakob SM (2017) High-resolution Respirometry to Assess Mitochondrial Function in Permeabilized and Intact Cells. J Vis Exp 54985. https://doi.org/10.3791/54985

85. Kong JY, Rabkin SW (1999) Thapsigargin enhances camptothecin-induced apoptosis in cardiomyocytes. Pharmacol Toxicol 85:212–220. https://doi.org/10.1111/j.1600-0773.1999.tb02011.x

86. Duchen MR (2000) Mitochondria and calcium: from cell signalling to cell death. J Physiol 529:57–68. https://doi.org/10.1111/j.1469-7793.2000.00057.x

87. Bugger H, Pfeil K (2020) Mitochondrial ROS in myocardial ischemia reperfusion and remodeling. Biochimica et Biophysica Acta (BBA) - Molecular Basis of Disease 1866:165768. https://doi.org/10.1016/j.bbadis.2020.165768

88. Mishra PK, Adameova A, Hill JA, et al (2019) Guidelines for evaluating myocardial cell death. Am J Physiol Heart Circ Physiol 317:H891–H922. https://doi.org/10.1152/ajpheart.00259.2019

89. Heusch G (2020) Myocardial ischaemia–reperfusion injury and cardioprotection in perspective. Nat Rev Cardiol 17:773–789. https://doi.org/10.1038/s41569-020-0403-y

90. Tixeira R, Caruso S, Paone S, et al (2017) Defining the morphologic features and products of cell disassembly during apoptosis. Apoptosis 22:475–477. https://doi.org/10.1007/s10495-017-1345-7

91. Ziegler U, Groscurth P (2004) Morphological features of cell death. News Physiol Sci 19:124–128. https://doi.org/10.1152/nips.01519.2004

92. Lee DY, Lee K-S, Lee HJ, et al (2008) Kynurenic acid attenuates MPP+-induced dopaminergic neuronal cell death via a Bax-mediated mitochondrial pathway. European Journal of Cell Biology 87:389–397. https://doi.org/10.1016/j.ejcb.2008.03.003

93. Meller R, Schindler CK, Chu XP, et al (2003) Seizure-like activity leads to the release of BAD from 14-3-3 protein and cell death in hippocampal neurons in vitro. Cell Death Differ 10:539–547. https://doi.org/10.1038/sj.cdd.4401206

94. Peng T-I, Jou M-J (2010) Oxidative stress caused by mitochondrial calcium overload. Ann N Y Acad Sci 1201:183–188. https://doi.org/10.1111/j.1749-6632.2010.05634.x

95. Smaili SS, Hsu YT, Youle RJ, Russell JT (2000) Mitochondria in Ca2+ signaling and apoptosis. J Bioenerg Biomembr 32:35–46. https://doi.org/10.1023/a:1005508311495

96. Montes de Oca Balderas P, Aguilera P (2015) A Metabotropic-Like Flux-Independent NMDA Receptor Regulates Ca2+ Exit from Endoplasmic Reticulum and Mitochondrial Membrane Potential in Cultured Astrocytes. PLoS One 10:e0126314. https://doi.org/10.1371/journal.pone.0126314

97. Kwong JQ, Molkentin JD (2015) Physiological and pathological roles of the mitochondrial permeability transition pore in the heart. Cell Metab 21:206–214. https://doi.org/10.1016/j.cmet.2014.12.001

98. Javadov S, Chapa-Dubocq X, Makarov V (2018) Different approaches to modeling analysis of mitochondrial swelling. Mitochondrion 38:58–70. https://doi.org/10.1016/j.mito.2017.08.004

99. Federico M, Portiansky EL, Sommese L, et al (2017) Calcium-calmodulin-dependent protein kinase mediates the intracellular signalling pathways of cardiac apoptosis in mice with impaired glucose tolerance. J Physiol 595:4089–4108. https://doi.org/10.1113/JP273714

100. Karbowski M, Youle RJ (2003) Dynamics of mitochondrial morphology in healthy cells and during apoptosis. Cell Death Differ 10:870–880. https://doi.org/10.1038/sj.cdd.4401260

101. Yang M, Linn BS, Zhang Y, Ren J (2019) Mitophagy and mitochondrial integrity in cardiac ischemia-reperfusion injury. Biochim Biophys Acta Mol Basis Dis 1865:2293–2302. https://doi.org/10.1016/j.bbadis.2019.05.007

102. Atici AE, Crother TR, Noval Rivas M (2023) Mitochondrial quality control in health and cardiovascular diseases. Front Cell Dev Biol 11:1290046. https://doi.org/10.3389/fcell.2023.1290046

103. Rafelski SM (2013) Mitochondrial network morphology: building an integrative, geometrical view. BMC Biol 11:71. https://doi.org/10.1186/1741-7007-11-71

104. Glancy B, Kim Y, Katti P, Willingham TB (2020) The Functional Impact of Mitochondrial Structure Across Subcellular Scales. Front Physiol 11:541040. https://doi.org/10.3389/fphys.2020.541040

105. Cogliati S, Enriquez JA, Scorrano L (2016) Mitochondrial Cristae: Where Beauty Meets Functionality. Trends Biochem Sci 41:261–273. https://doi.org/10.1016/j.tibs.2016.01.001

106. Kalogeris T, Baines CP, Krenz M, Korthuis RJ (2012) Cell biology of ischemia/reperfusion injury. Int Rev Cell Mol Biol 298:229–317. https://doi.org/10.1016/B978-0-12-394309-5.00006-7

107. Zorov DB, Juhaszova M, Sollott SJ (2006) Mitochondrial ROS-induced ROS release: an update and review. Biochim Biophys Acta 1757:509–517. https://doi.org/10.1016/j.bbabio.2006.04.029

108. Wu M-Y, Yiang G-T, Liao W-T, et al (2018) Current Mechanistic Concepts in Ischemia and Reperfusion Injury. Cell Physiol Biochem 46:1650–1667. https://doi.org/10.1159/000489241

109. Poles MZ, Nászai A, Gulácsi L, et al (2021) Kynurenic Acid and Its Synthetic Derivatives Protect Against Sepsis-Associated Neutrophil Activation and Brain Mitochondrial Dysfunction in Rats. Front Immunol 12:717157. https://doi.org/10.3389/fimmu.2021.717157

110. Sharmin O, Abir AH, Potol A, et al (2020) Activation of GPR35 protects against cerebral ischemia by recruiting monocyte-derived macrophages. Sci Rep 10:9400. https://doi.org/10.1038/s41598-020-66417-8

111. Chen K, He L, Li Y, et al (2020) Inhibition of GPR35 Preserves Mitochondrial Function After Myocardial Infarction by Targeting Calpain 1/2. J Cardiovasc Pharmacol 75:556–563. https://doi.org/10.1097/FJC.0000000000000819

112. Wu Y, Zhang P, Fan H, et al (2023) GPR35 acts a dual role and therapeutic target in inflammation. Front Immunol 14:1254446. https://doi.org/10.3389/fimmu.2023.1254446

113. Turski WA, Małaczewska J, Marciniak S, et al (2014) On the toxicity of kynurenic acid in vivo and in vitro. Pharmacol Rep 66:1127–1133. https://doi.org/10.1016/j.pharep.2014.07.013

114. Braidy N, Grant R, Brew BJ, et al (2009) Effects of Kynurenine Pathway Metabolites on Intracellular NAD Synthesis and Cell Death in Human Primary Astrocytes and Neurons. Int J Tryptophan Res 2:61–69. https://doi.org/10.4137/ijtr.s2318

115. Papp A, Hartwell R, Evans M, Ghahary A (2018) The Safety and Tolerability of Topically Delivered Kynurenic Acid in Humans. A Phase 1 Randomized Double-Blind Clinical Trial. J Pharm Sci 107:1572–1576. https://doi.org/10.1016/j.xphs.2018.01.023

Links:

Web 1: https://www.who.int/news-room/fact-sheets/detail/the-top-10-causes-of-death

Acknowledgements

I would like to express my sincere appreciation and gratitude to my supervisor, Dr. Renáta Molnár-Gáspár as well as to my former supervisor, Dr. Tamás Csont (MEDICS Research Group, Department of Biochemistry, Albert Szent-Györgyi Medical School, University of Szeged) for the support and guidance they provided throughout my doctoral work. Their mentorship and expertise have been instrumental in my academic and personal growth.

I would like to thank Prof. Dr. Norbert Jost and Prof. Dr. László Dux for providing me with the possibility to complete my doctoral work at the Doctoral School of Multidisciplinary Sciences, as well as to the University of Szeged for providing me with a doctoral scholarship.

I deeply appreciate the support I received from Prof. Dr. Zita Borbényi and my colleagues from the Division of Hematology, Albert Szent-Györgyi Health Centre, University of Szeged.

I would like to express my special thanks for all the help and work of the members of the Metabolic Diseases and Cell Signaling Research Group. I am especially grateful for the contributions of Dr. Barbara Erdélyi-Furka, Éva Plechl, Dóra Csóré, as well as for the work of my former undergraduate students, Mirjam Anka and Raissa Guedes Pereira. Without their professional help, teamwork and the inspiring and friendly atmosphere they created, this thesis would not have been possible to write.

I would like to express my gratitude to our collaborative partners, Nóra Igaz, Mónika Kiricsi, László Juhász, Marietta Poles, Bernát Nógrádi and Tamás Ferenc Polgár.

I would also like to thank to Prof. Dr. László Vécsei for providing me with the possibility to join the collaborative research project aiming to investigate the effects of kynurenines.

Last but not least, I would like to express my sincerest gratitude to my family and friends. I am deeply grateful for all the encouragement, support, patience and love I received from my husband, Bernát - his belief in my capabilities always helped me along this journey. I am also grateful to my mother and father, other family members, as well as to my friends, especially to Abigél, Barbi and Fanni, for the motivation and help they provided me with. This accomplishment is just as much theirs as it is mine.

This work was financially supported by the projects GINOP-2.3.2-15-2016-00034, EFOP-3.6.2-16-2017-00006 (LIVE LONGER), 20391-3/2018/FEKUSTRAT and by the OTKA-NKFIH (FK138992), OTKA-NKFIH (K143889), OTKA-NKFIH (K142371), TKP2021-EGA-32.